

1 Cysteine-Rich Positions Outside the Structural Zinc Motif of Human 2 Papillomavirus E7 Provide Conformational Modulation and Suggest 3 Functional Redox Roles

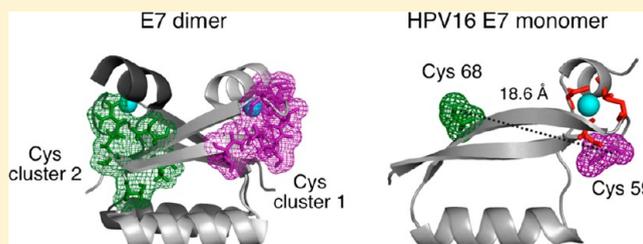
4 Lucía B. Chemes,^{†,§} Gabriela Camporeale,^{†,§} Ignacio E. Sánchez,[‡] Gonzalo de Prat-Gay,^{*,†}
5 and Leonardo G. Alonso^{*,†}

6 [†]Protein Structure–Function and Engineering Laboratory, Fundación Instituto Leloir and IIBBA-CONICET, Av. Patricias Argentinas
7 435, 1405 Buenos Aires, Argentina

8 [‡]Protein Physiology Laboratory, Departamento de Química Biológica, Facultad de Ciencias Exactas y Naturales and
9 IQUIBICEN-CONICET, Universidad de Buenos Aires, C1428EGA Buenos Aires, Argentina

10 **S** Supporting Information

11 **ABSTRACT:** The E7 protein from high-risk human papil-
12 lomavirus is essential for cell transformation in cervical,
13 oropharyngeal, and other HPV-related cancers, mainly through
14 the inactivation of the retinoblastoma (Rb) tumor suppressor.
15 Its high cysteine content (~7%) and the observation that
16 HPV-transformed cells are under oxidative stress prompted us
17 to investigate the redox properties of the HPV16 E7 protein
18 under biologically compatible oxidative conditions. The seven
19 cysteines in HPV16 E7 remain reduced in conditions
20 resembling the basal reduced state of a cell. However, under oxidative stress, a stable disulfide bridge forms between cysteines
21 59 and 68. Residue 59 has a protective effect on the other cysteines, and its mutation leads to an overall increase in the oxidation
22 propensity of E7, including cysteine 24 central to the Rb binding motif. Glutathionylation of Cys 24 abolishes Rb binding, which
23 is reversibly recovered upon reduction. Cysteines 59 and 68 are located 18.6 Å apart, and the formation of the disulfide bridge
24 leads to a large structural rearrangement while retaining strong Zn association. These conformational and covalent changes are
25 fully reversible upon restoration of the reductive environment. In addition, this is the first evidence of an interaction between the
26 N-terminal intrinsically disordered and the C-terminal globular domains, known to be highly and separately conserved among
27 human papillomaviruses. The significant conservation of such noncanonical cysteines in HPV E7 proteins leads us to propose a
28 functional redox activity. Such an activity adds to the previously discovered chaperone activity of E7 and supports the picture of a
29 moonlighting pathological role of this paradigmatic viral oncoprotein.



30 **H**uman papillomaviruses (HPV) have drawn the attention
31 of the scientific community since the discovery of their
32 direct involvement in human cancer development.^{1,2} Over 100
33 papillomavirus types that infect humans have been described,³
34 only a subset of which possess oncogenic potential and have been
35 classified as “high-risk” types.² As opposed to high risk HPVs,
36 many HPV types produce benign lesions and are classified as
37 “low risk”.² Moreover, most HPV infections are self-limited and
38 resolve without clinical manifestation.⁴ In fact, HPV-induced
39 neoplastic lesions do not produce infective particles and can be
40 considered as unproductive events in the HPV life cycle.⁵

41 In order to produce infective particles, the HPV genome must
42 replicate within a stratified epithelium, and as HPVs are devoid of
43 the enzymatic machinery required to duplicate their genome,
44 these viruses must use the host DNA replication machinery to
45 generate new infective viruses.⁶ Most papillomaviruses infect
46 basal undifferentiated cells of stratified skin and mucous epithelia,
47 where the genome is initially amplified and maintained at low
48 copy number, but subsequent viral replication takes place in
49 differentiating keratinocytes, which have withdrawn from the cell

cycle. The HPV genome codes for a handful of proteins that act
50 in a coordinate manner to override the control mechanisms that
51 strictly regulate the host cell cycle.⁷ This complex task depends
52 largely on the E7 oncoprotein, which is essential for stimulating
53 S-phase reentry in differentiating keratinocytes, producing an
54 uncoupling of proliferation and differentiation in these cells.⁸
55 According to the experimental evidence obtained from the
56 prototypical E7 protein from the HPV16 type (HPV16 E7), E7-
57 related functions are mediated by its ability to interact with
58 multiple cellular targets.^{9,10} The retinoblastoma protein (Rb)
59 was the first cellular target identified for the E7 protein.¹¹ High
60 affinity binding of E7 to Rb is required for the transforming
61 properties of the high-risk HPV16 E7 protein in transfected
62 cells,¹² and it is the primary and best-characterized interaction
63 related to HPV-mediated cellular transformation.¹³ Rb binding is
64 a property shared by both high- and low-risk HPVs.¹⁴ Persistent
65

Received: November 21, 2013

Revised: February 5, 2014



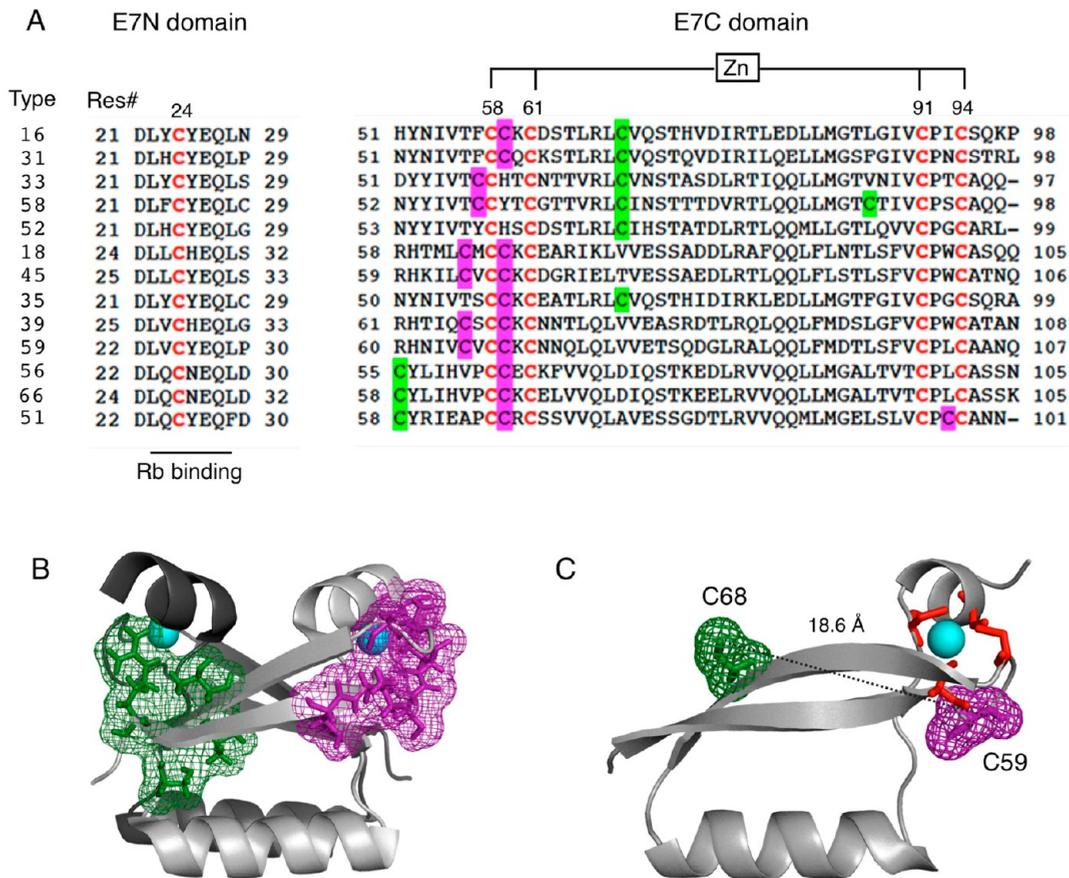


Figure 1. Distribution of cysteine-rich positions in the E7 oncoprotein. (A) Alignment of 13 high-risk E7 sequences. A portion of the E7N and the entire E7C domain are shown. Canonical cysteine residues involved in Rb binding and Zn coordination are shown in red, while noncanonical cysteines located in Cluster 1 and Cluster 2 regions in E7C are indicated in pink and green, respectively. The 10 Cys-rich positions previously identified in 219 papillomavirus E7C sequences²⁵ are indicated below the alignment; pink circles: Cluster 1 positions; green circles: Cluster 2 positions. (B) Structure of the HPV45 E7 dimer (PDB id: 2F8B) showing the location of Cluster 1 (pink sticks) and Cluster 2 (green sticks) Cys-rich positions in one E7 monomer. Cyan spheres: Zn atoms. Each monomer in the homodimer is represented in light and dark gray, respectively. Cluster 1 positions are close to the Zn coordination site of the same monomer, while Cluster 2 positions are close in space to the Zn coordination site of the opposite monomer. (C) Model structure of the HPV16 E7 monomer obtained using Modeler and the HPV45 E7 monomer as a template (PDB id: 2EWL) (see Materials and Methods). Cyan sphere: Zn atom; red sticks: Zn-coordinating cysteines; pink sticks: noncanonical cysteine 59 residue; green sticks: noncanonical cysteine 68 residue. The distance between the -SH groups of cysteines 59 and 68 is indicated.

66 expression of the HPV16 E7 protein is required for maintenance
 67 of the transformed phenotype.¹⁵ It has been described that
 68 HPV16-positive cervical cancer lesions show a higher oxidative
 69 environment than normal noninfected tissues and a marked
 70 down-regulation of antioxidant enzymes such as superoxide
 71 dismutase, catalase, and glutathione peroxidase.^{16–18} Moreover,
 72 it was shown that the sole expression of HPV16 E7 in HaCaT
 73 keratinocytes induces oxidative stress.¹⁹
 74 HPV16 E7 is a small acidic 98-amino-acid protein²⁰ with two
 75 distinct structural domains, the globular C-terminal domain
 76 (E7C) for which X-ray and NMR structures have been solved for
 77 HPV types 1 and 45^{21,22} and the intrinsically disordered N-
 78 terminal domain (E7N IDD), which is extended in solution and
 79 lacks canonical secondary and tertiary structure elements.²³
 80 Although high-resolution structures show a homodimeric
 81 arrangement for the E7C domain,²² E7 shows a complex
 82 hydrodynamic behavior in solution and exhibits multiple
 83 monomerization–dimerization–oligomerization equilibria with
 84 a reported dimer dissociation constant of ~1 μM.²⁴ HPV16 E7
 85 presents seven cysteine residues in its sequence, five of which
 86 have a strict or very high conservation degree across HPVs²⁵
 87 (Figure 1A). HPV16 E7 binds one Zn atom per monomer

through a tetra-cysteine coordination site located in the globular
 E7C domain²⁶ (Figure 1A). Metal coordination is essential for
 maintaining the structural integrity of the protein, and metal loss
 leads to the formation of large spherical soluble oligomers
 (E7SOs).²⁷ The four cysteine positions corresponding to the
 tetra-cysteine Zn binding motif, CxxC-29aa-CxxC (positions 58,
 61, 91, and 94 in the HPV16 E7 sequence) are strictly conserved
 across human and animal papillomavirus types.²⁵ A fifth highly
 conserved cysteine residue (85% occurrence) corresponds to
 position 24 in the HPV16 E7 sequence and is located in the IDD
 E7N domain within a short linear motif responsible for Rb
 binding that spans residues 21–29 (DLYC**Y**EQLN)²⁵ (Figure
 1A). A quantitative investigation of the interaction mechanism
 between the HPV16 E7 protein and the RbAB domain in
 solution revealed that 90% of the binding energy is provided by
 the LxCxE motif, with an additional binding determinant located
 in the E7C domain, establishing a dual-contact mode.²⁸ Cysteine
 24 in HPV16 E7 is located in the IDD domain and hence is highly
 exposed to the solvent and to oxidative agents, which are present
 in dysplastic and neoplastic tissues that are under oxidative
 stress.¹⁶ The redox regulation of this fundamental cysteine and

109 the consequences of its oxidation on Rb binding remain
110 unknown so far.

111 On the basis of its high cysteine content, HPV16 E7 can be
112 considered as a cysteine-rich protein, with seven out of 98
113 residues (~7%) corresponding to this amino acid, a proportion
114 well above the overall average content for mammalian proteins
115 (2.3%²⁹). Recently, a detailed study on the sequence evolution of
116 the globular homodimeric E7C domain based on the alignment
117 of 219 papillomavirus sequences led us to identify 10 cysteine-
118 rich positions within the E7 sequence in addition to the canonical
119 cysteines involved in Zn and Rb binding. Despite presenting
120 fairly low degrees of conservation, these noncanonical positions
121 exhibit at least 5.9% cysteine abundance, 4-fold above the average
122 percentage reported in UniProt (Figure 1A).²⁵ About 70% of E7
123 sequences possess at least one noncanonical cysteine occupying
124 one of these ten positions, and 30% of E7 sequences present two
125 noncanonical cysteines.²⁵ These noncanonical cysteine-rich
126 positions can be classified in two clusters that differ in their
127 relative orientation with respect to the Zn binding sites of each
128 monomer.²⁵ Cluster 1 positions (residues 56, 57, 59, 60, 63, and
129 98 of the HPV16 E7 sequence) are close in sequence to the Zn
130 binding site of the same monomer, while Cluster 2 positions
131 (residues 51, 68, 69, and 71 in HPV16 E7) are distant in
132 sequence from the Zn binding site of the same monomer but are
133 spatially proximal to the Zn binding site of the second monomer
134 in the structure of the E7 dimer (Figure 1B). HPV16 E7 presents
135 two noncanonical extra cysteines in addition to those involved in
136 Zn and Rb binding, located at positions 59 (Cluster 1, magenta)
137 and 68 (Cluster 2, green) (Figure 1C).²⁵ Strong epidemiological
138 evidence indicates that 13 papillomavirus types (HPV types 31,
139 33, 35, 39, 45, 51, 52, 56, 58, 59, and 66) are considered high risk
140 for the development of cervical cancer and therefore are
141 considered of clinical relevance.³⁰ With the exception of HPV
142 52, all E7 proteins from this group of high-risk types contain at
143 least two noncanonical cysteines in their sequence (Figure 1A).

144 The importance of the cysteine residue is based on its
145 particular chemical behavior, due to the presence of the ionizable
146 thiol group, which is an excellent nucleophile at neutral pH.^{31,32}
147 This reactivity makes cysteine a likely target for chemical redox
148 modifications that often lead to redox-regulation of protein
149 function.^{33–35} Cysteine can suffer many chemical modifications
150 that include reversible changes such as the formation of disulfide
151 bridges, glutathionylation,^{36,37} and sulfenic acid formation,³⁴ as
152 well as often irreversible changes such as sulfinic and sulfonic acid
153 formation.^{38,39} The oxidation agent and redox potentials that
154 trigger cysteine modification within the cell are finely tuned and
155 depend largely on the structural context of the reactive
156 cysteines.⁴⁰ As an example, while the equilibrium oxidation
157 constant for the formation of an intramolecular disulfide bridge
158 between adjacent cysteines present in the CXXC motif of folded
159 thioredoxin is 10^{-16} M,⁴¹ the equilibrium oxidation constant for
160 formation of an intramolecular disulfide bridge in the urea-
161 unfolded thioredoxin is 0.026 M.⁴¹

162 The reactivity of the thiol group and the high prevalence of
163 noncanonical cysteines in E7 proteins from clinically relevant
164 HPV strains, together with the fact that HPV transformed tissues
165 own high levels of oxidative stress, suggest a previously
166 undescribed functional role for the noncanonical cysteines
167 present within the E7 sequence. In the present work, we assessed
168 the redox regulation and chemical reactivity of cysteines in the
169 high-risk HPV16 E7 protein and their consequences on E7
170 structure and conformation, by using a combination protein
171 mutagenesis, spectroscopy, and mass spectrometry techniques.

■ MATERIALS AND METHODS

172

Protein Expression and Purification and Peptide
Synthesis. The E7 wild type protein from the HPV 16 strain
174 was obtained as described earlier.²⁰ Briefly, HPV 16 E7 was
175 cloned as a thrombin-cleavable fusion protein downstream of the
176 maltose binding protein (MBP) in a p-MALc2 vector (New
177 England Biolabs) and expressed in the *E. coli* TB1 strain. After
178 cleavage of the MBP-E7 fusion protein with protease, the isolated
179 E7 protein was obtained containing two extra amino acids
180 (glycine and serine) at the amino terminus due to the engineered
181 thrombin cleavage site. The HPV 16 E7 protein was also cloned
182 into a PTZ18u vector under the T7 promoter downstream to a
183 short peptide (19 aa) of the β -galactosidase protein. An
184 enterokinase (EK) cleavage site with the sequence DDDDK
185 was inserted between the peptide and the amino terminus of the
186 E7 protein. The cysteine mutants on the E7 HPV16 protein were
187 obtained by site-directed, inverse polymerase chain reaction
188 mutagenesis of the PTZ18u E7 HPV16 plasmid, used as a
189 template. For this purpose, primers were synthesized containing
190 the desired cysteine to alanine substitution (Integrated DNA
191 Technologies). The obtained PCR fragment containing the
192 mutation was ligated, and the resulting plasmid was sequenced in
193 order to confirm the desired mutation and then transformed into
194 BL21(DE3) *E. coli* strain for expression. By using the EK
195 protease we obtained the E7 mutant proteins with the free N-
196 terminus without the addition of any extra amino acid. Inclusion
197 bodies (IBs) containing HPV-16 E7 mutants were purified as
198 described.²⁷ The final step in the purification of E7 wild type and
199 mutant proteins is always a size exclusion chromatography in a
200 Superdex 75 column (GE Healthcare Bio-Sciences Corp, USA)
201 that is performed in 10 mM sodium phosphate, pH 7.0 buffer
202 without the addition of any reductant agent (DTT or 2-
203 mercaptoethanol would interfere in subsequent analytical
204 determinations of the protein oxidation state). Concentrated
205 stock proteins without the addition of any reductant were
206 maintained at -80 °C during 3 months without any appreciable
207 oxidative damage of the sample. The expression and purity of the
208 purified proteins were checked by 15% SDS-PAGE Coomassie
209 blue stained.⁴² All proteins presented 90% purity and no more
210 than 10% of oxidized dimeric species. To obtain oxidized
211 E7desLxCxE, a solution containing 50 μ M of protein in 10 mM
212 potassium phosphate buffer and 5 mM total glutathione
213 concentration with a GSH/GSSG ratio of 0.1, pH 7.5, was
214 incubated 80 min at 37°C. After confirming by RP-HPLC that the
215 oxidized species reached not less than 78%, the sample was
216 desalted in a PD-10 column (GE Healthcare Bio-Sciences Corp,
217 USA) equilibrated with 10 mM potassium phosphate buffer, pH
218 7.5. Oxidized E7desLxCxE protein was concentrated up to 20
219 μ M and stored at -80 C.
220

The N-terminal peptide spanning the first 40 amino acids of
221 the E7 HPV16, which includes the cysteine 24, was obtained by
222 chemical synthesis at the W. M. Keck Facility (Yale University,
223 New Haven, CT) with the N-terminal acetylated and C-terminal
224 amidation.
225

Colorimetric Determination of Zn and Thiol Titration.
226 Zinc release by thiol titration was determined spectrophoto-
227 metrically by the measurement of the metallochromic indicator
228 PAR.⁴³ Purified E7 wild type protein at a concentration of 5 μ M
229 was incubated with PAR (100 μ M) in 50 mM potassium
230 phosphate buffer, pH 7.5 at RT. Under this condition, only soft-
231 bound metal or adventitious metal is determined because the
232 constant affinity for Zn of the E7 protein is higher than the PAR-
233

Zn constant affinity and structural tetrahedrally coordinated Zn is not transferred to PAR. By adding quantified aliquots of the organomercury agent PMPS, which readily react with sulfhydryls in proteins, Zn is released from E7 protein, and the reaction was monitored at 500 nm. The exact metal content was determined from a calibration curve using a Zn standard solution (Sigma, St Louis, MO).

Thiol titration was performed by adding successive quantified aliquots of PMPS to a 5 μ M E7 wild type protein in 50 mM potassium phosphate buffer, pH 7.5 at RT. The reaction of PMPS with the thiol group of cysteines is followed at 250 nm.

The Zn content of E7 mutants was evaluated by adding PMPS to a final concentration of 100 μ M to a sample containing 3 μ M concentration of each protein and 100 μ M PAR in 50 mM potassium phosphate buffer, pH 7.5. The formation of PAR-Zn complexes was assessed by following the time trace at 500 nm. The addition of an excess of DTT (250 μ M final concentration) displaces the PMPS from the protein (DTT provides an excess of reactive thiol groups) and allows the protein to reup take Zn. Due to the high affinity of the E7 proteins for Zn, the addition of DTT leads to a decrease in the absorbance at 500 nm (i.e., the PAR-Zn complexes are dissolved).

Quantitative Thiol Determination by DTNB. A sample containing 3 μ M protein in 50 mM phosphate buffer pH 7.5 and 0.25 mM DTNB was incubated for 5–10 min, and the absorbance at 412 nm was obtained.⁴⁴ A calibration curve was done using reduced glutathione (GSH) as standard.

Determination of Redox Equilibria in Glutathione Buffer and H₂O₂ Oxidation. The redox equilibria of the E7 wild type and cysteine mutants was assessed by incubating a protein solution with different reduced and oxidized glutathione ratios (N), where N is $[GSH]/[GSSG]$ at a constant total glutathione concentration. For each evaluated protein, a curve was obtained by incubating 250 μ L of a solution containing 15 μ M E7, 5 mM final glutathione concentration with different N ratio in 50 mM potassium phosphate buffer, pH 7.5 at 8 °C overnight (18 h). To stop redox reaction, 200 μ L of GdmCl 6.0 M and 0.1% TFA were added to E7 samples. The identification of the oxidized species and the quantitative analysis of the reduced and oxidized species in E7 wild type and cysteine mutants were performed by reverse phase HPLC (RP-HPLC) using a C₄ column, 250 mm \times 4.6 mm (Bio-Basic-C4, Thermo Scientific, PA, USA). The eluted species were detected at 220 nm using an isocratic step at 20% (v/v) acetonitrile/water 0.1% TFA for 10 min and a gradient step from 20% to 70% (v/v) acetonitrile/water 0.1% TFA in 25 min. The oxidation of E7 wild type with hydrogen peroxide was performed by incubating 250 μ L of a solution containing 15 μ M E7 in 50 mM potassium phosphate buffer, pH 7.5 for 30 min at 37 °C with 150 μ M of H₂O₂. The reaction was stopped by adding 200 μ L of GdmCl 6.0 M, 0.1% TFA, and 5 mM methionine.

The analysis of the redox equilibrium in glutathione buffer of the N-terminal peptide (1–40) was performed using a different RP-HPLC method using a C₁₈ column, 250 mm \times 4.6 mm (Bio-Basic-C18, Thermo Scientific, PA, USA). The eluted species were detected at 220 nm by an isocratic step from 10% (v/v) acetonitrile/water 0.1% TFA for 10 min and a gradient step from 10% to 50% (v/v) acetonitrile/water 0.1% TFA in 30 min. The reduced fraction at each N ratio was calculated by integrating both the area under the peak corresponding to the reduced species and the total peak area (all peaks). The equilibrium constant (K_{mix}) for the formation of a mixed disulfide bridge

between the cysteine 24 and the glutathione was calculated by fitting the reduced fraction to the following equation:

$$\text{RF} = \left[\frac{1}{(K_{\text{mix}}/N) + 1} \right] + b \quad (1)$$

where RF is the reduced fraction, K_{mix} is the equilibrium constant for the reaction of disulfide formation between a protein cysteine (P(SH)) and glutathione according to the following equilibrium:



N is the ratio between GSH and GSSG, and b is a constant that corrects for a protein population that is refractive to oxidation.

Intact Protein Analysis and Identification of Cysteine Connectivity by MALDI-TOF. MALDI-TOF mass spectrometry of intact protein was performed by diluting 1/5 v/v aliquots of the E7 samples in oversaturated solution of sinapinic acid in 30/70/0.1% (v/v) acetonitrile/water/TFA. A 1- μ L aliquot of the sample was spotted onto a AnchorChip (Bruker, Billerica, MA, USA) and left to crystallize by air-drying. Samples were analyzed on a Bruker Microflex MALDI-TOF (Bruker, Billerica, MA, USA). Identification of cysteine connectivity in E7desLxCxE oxidized sample was performed by treating a protein solution (ca. 20–50 μ M) with 56 mM iodoacetamide (IAA) in 50 mM Tris-HCl, pH 8.0 for 30 min at room temperature in a dark place in order to block reactive sulfhydryls. *N*-Ethylmaleimide (NEM) cysteine alkylation was performed by treating a protein solution (ca. 20–50 μ M) with 30 mM NEM in 50 mM phosphate buffer, pH 8.0 for 30 min at room temperature in a dark place in order to block reactive sulfhydryls. The sample was precipitated by adding 10% v/v TCA on ice, and after centrifugation at 9000g for 30 min the supernatant was discarded and the sample was washed twice with cold acetone and left to dry. Pellet was resuspended with 50 mM Tris-HCl, 5 mM octyl β -D-glucopyranoside (OPG), pH 8.0 containing sequencing grade trypsin (Sigma, St Louis, MO) at 1/10 (w/w). When reductant was required, 5 mM concentration of ultrapure DTT was added to the reaction. Proteolysis was left to proceed for 18 h at 8 °C, and then the reaction was stopped by the addition of TFA to 0.1% final concentration. A 1- μ L aliquot was spotted onto a AnchorChip (Bruker, Billerica, MA, USA), and 1 μ L of oversaturated solution of α -cyano-4-hydroxycinnamic acid (HCCA) in 30/70/0.1% (v/v) acetonitrile/water/TFA was loaded to the protein sample. Samples were analyzed on a Bruker Microflex MALDI-TOF.

Binding of Reduced and Oxidized E7N to the RbAB Domain. Experiments were performed as described in ref 45. Briefly, the E7N peptide (1–2 mg) was labeled at its amino terminus with 1.5 mg/mL fluorescein isothiocyanate (FITC) in 100 mM sodium carbonate buffer, pH 8 for 2 h at room temperature and separated from labeling reagents by a desalting column (PD-10, GE Healthcare) followed by RP-HPLC. Oxidation of FITC-labeled E7N was performed as described, and the labeled and oxidized peptides were further purified by RP-HPLC. The purity of all preparations was evaluated by MALDI-TOF spectroscopy. Measurements were performed in a Jasco FP6500 fluorescence polarimeter assembled in L geometry, using excitation and emission wavelengths of 495 and 520 nm, with 3–5 nm bandwidth. All measurements were performed at 20 \pm 0.1 °C in 20 mM sodium phosphate buffer, pH 7, 200 mM NaCl, and 0.1% Tween-20. For titration, increasing amounts of a concentrated solution of RbAB protein were added to a cuvette containing 100 nM FITC-labeled E7N peptide. Only for testing binding of reduced E7N to RbAB, 2 mM DTT was added to the

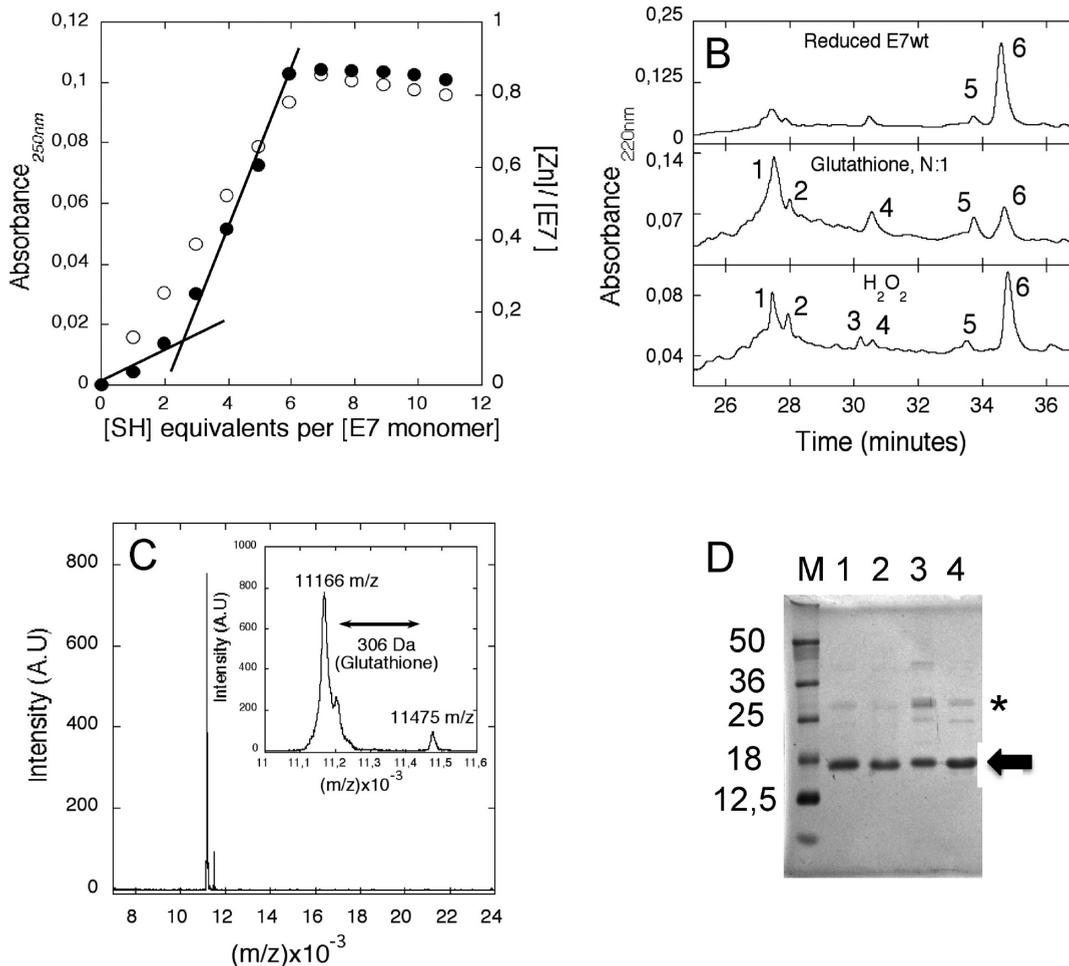


Figure 2. Basal redox state and oxidation behavior of the E7wt protein. (A) Cysteine sulphydryl titration and Zn release of purified E7wt protein. Cysteine residues were titrated by the addition of PMPS, and the formation of thiol-mercuric bonds was followed by recording the absorbance at 250 nm (open circles). In an independent experiment, Zn release from E7wt was induced by the addition of PMPS, and released Zn was detected by the colorimetric reagent PAR to obtain the Zn to protein molar ratio (full circles). The x-axis represents the ratio of PMPS [SH] molar equivalents per E7 monomer molar equivalents. (B) Effect of different oxidation agents on the E7wt protein analyzed by RP-HPLC. Upper panel: RP-HPLC chromatogram of the E7wt protein incubated for 18 h with glutathione at a [GSH]:[GSSG] ratio of N:1000 (reducing conditions). Middle panel: RP-HPLC chromatogram of the E7wt protein incubated for 18 h with glutathione at a ratio of N:1 (oxidative conditions). Bottom panel: RP-HPLC chromatogram of the E7wt protein incubated for 18 h with 0.15 mM of H₂O₂. E7wt concentration was 15 μM. Peaks are identified with a number according to their order of elution in the chromatogram, with peak 6 corresponding to the fully reduced protein. (C) MALDI-TOF spectrum of the E7wt protein incubated with glutathione at ratio of N:1. Inset, detail of the major peak and mixed disulfide peak areas. (D) SDS-PAGE of the E7wt protein. Lane M: molecular weight markers expressed in kDa. Lane 1: E7wt oxidized with glutathione at a ratio of N:1. Lane 2: reduced stock E7wt sample. Lane 3: E7wt oxidized plus the addition of IAA in the cracking buffer. Lane 4: reduced stock E7wt sample plus the addition of IAA in the cracking buffer. Arrow, major monomeric E7wt species found; *, minor dimeric E7wt species.

354 buffer solution. Samples were allowed to equilibrate for at least 2
 355 min in order to ensure that measurements were performed at
 356 steady state.

357 **Data Analysis and Fitting.** In order to obtain the K_D values
 358 for each interaction, the anisotropy values as a function of RbAB
 359 concentration were fit to the quadratic equation

$$Y = Y_F + \frac{(Y_B - Y_F) \cdot P_o}{(x + P_o + K_D) + \sqrt{(x + P_o + K_D)^2 - (4P_o x)}}$$

360 where Y_F and Y_B are the signal of free and bound peptide, K_D is
 361 the dissociation constant, and P_o is the total peptide
 362 concentration. Data fitting was performed with ProFit
 363 (Quantumsoft, Zurich). To test whether reduction of the

oxidized E7N yielded a species competent for RbAB binding, 364
 the reaction mixture obtained at the end point of the titration 365
 (100 nM oxidized FITC-E7N and 1 μM RbAB) was reduced by 366
 the addition of 5 mM DTT and the fluorescence anisotropy was 367
 followed over time. 368

Circular Dichroism (CD) and Fluorescence Spectroscopy. 369
 CD measurements were carried out on a Jasco J-810 370
 spectropolarimeter (Jasco, Easton, MD) employing a scan speed 371
 of 20 nm/min, a band-pass of 1 nm, and average response time of 372
 4 s. All spectra were an average of at least 5 scans. Temperature 373
 was maintained constant using a Peltier temperature-controlled 374
 sample compartment. Spectra of reduced and oxidized E7 at a 375
 concentration of 10 μM were taken on 0.1 cm path length cells in 376
 10 mM potassium phosphate buffer, pH 7.5. Fluorescence 377
 emission scans were taken on a FP-6500 spectrofluorometer 378
 (Jasco, Easton, MD). 379

380 **E7 Sequence Analysis, Modeling, and Cysteine**
381 **Exposure Calculations. Alignments.** Alignments for high
382 risk HPV E7 protein sequences were performed using the
383 MUSCLE algorithm⁴⁶ and manually edited using the SeaView
384 software.

385 *Modeling of the HPV16 E7 Monomer.* Three-dimensional
386 models for the HPV16 E7 monomer were obtained by using
387 Modeler v9.7 (<http://salilab.org/modeller/>)^{47,48} using the
388 HPV45 E7 monomer structure (PDB id: 2EWL) as a template.
389 The model for the HPV16 E7 dimer was obtained by structural
390 alignment of HPV16E7 monomers to the HPV45 dimer
391 structure (PDB id: 2F8B) using the PyMol software ([http://](http://www.pymol.org/)
392 www.pymol.org/).

393 *Fractional Cysteine Exposure.* Raw solvent accessibility
394 values, measured in Å², for each residue in the HPV45 E7
395 structure (PDB id: 28FB) and in the HPV16 E7 model were
396 calculated by using the DSSP algorithm⁴⁹ implemented by the
397 Centre for Molecular and Biomolecular Informatics ([http://](http://www.cmbi.ru.nl/dssp.html)
398 www.cmbi.ru.nl/dssp.html). Raw accessibility values obtained
399 for each residue were normalized taking into account the
400 maximal accessibility for each aminoacid, also measured in Å².⁴⁹

401 ■ RESULTS

402 **Redox Behavior of Cysteine Residues in the E7 HPV16**
403 **Protein.** The HPV16 E7 protein was recombinantly expressed
404 to obtain a pure and conformationally homogeneous sample that
405 contains a tightly bound Zn atom per E7 monomer.²⁰ This
406 protein sample is routinely stored at pH 7.0 in mild reducing
407 conditions (1 mM DTT) for several months without
408 modifications in its oligomeric or redox state. However, the
409 oxidation state of each of the seven cysteine residues in HPV16
410 E7 had not been previously assessed. In order to address this
411 issue, a sulfhydryl titration was performed on a HPV16 E7 stock
412 sample lacking reductant using the organomercuric reagent
413 PMPS, which shows a high reactivity and selectivity for thiols.⁴³
414 The full-length wild type E7 protein stock (E7wt onward) was
415 stepwise titrated with quantified aliquots of PMPS and the
416 reaction followed by absorbance at 250 nm (Figure 2A). A linear
417 increase in absorbance was observed with the titration of seven
418 cysteine equivalents per E7 monomer, indicating that all cysteine
419 residues in the sample were reduced. Independent measure-
420 ments of PMPS-induced Zn-release were performed by pre-
421 incubating E7wt samples with the PAR reagent and following
422 PAR-Zn complex formation following PMPS addition by
423 absorbance at 500 nm. The titration of ca. seven cysteines by
424 PMPS was also required to produce the complete release of Zn
425 from the E7wt protein (Figure 2A).

426 However, the Zn release curve showed two different slopes,
427 with the titration of the first three sulfhydryl equivalents by
428 PMPS not leading to stoichiometric metal release. These results
429 could reflect the expected differences in reactivity of free
430 cysteines (CYS 24, 59, and 68), which account for the first slope,
431 and Zn-coordinating cysteines (CYS 58, 61, 91, and 93) that
432 account for the second slope. It should be noted that due to the
433 hydrophobic nature of PMPS, no differences in cysteine
434 reactivity based on their accessibility are expected.

435 Quantitative determination of the reactive cysteines with
436 DTNB yielded 6.3 ± 0.3 mol of cysteine per mole of protein (not
437 shown) in excellent agreement with the PMPS titration
438 experiments. MALDI-TOF analysis of the stock E7wt protein
439 yielded a main molecular ion mass $[M + H]^+$ of 11170.8 m/z ,
440 which can be assigned, considering the experimental error
441 (0.1%) to the monomeric E7 protein with an expected molecular

weight of 11167.5 Da (Supplementary Figure S1) for the fully
reduced protein. Moreover, the presence of oxidized dimeric or
oligomeric species was not observed. Altogether, these results
indicated that all seven cysteine residues in the stock E7wt
protein were in their reduced state. No evidence of protein
oxidation was observed during protein storage, despite the
absence of reductant in the storage buffer.

Next, we assessed the redox behavior of E7wt under oxidative
stress conditions using two biologically relevant oxidants:
glutathione and hydrogen peroxide. Glutathione is the main
redox buffer in the cell,⁵⁰ and varying the reduced over oxidized
glutathione (GSSG) ratio allows us to control the redox
potential,⁴¹ while the H₂O₂ molecule is a common although
rather nonspecific oxidant stimulus in living cells.⁵¹ The E7wt
stock solution incubated in reducing and oxidizing conditions
was resolved by RP-HPLC (see Materials and Methods). The
E7wt protein stock incubated overnight in a reducing condition
with a total glutathione concentration of 5 mM at a ratio of N :
[GSH]/[GSSG] of 1000 at 8 °C eluted as a main peak (peak 6)
at ~34.6 min (Figure 2B, upper panel) with minor low intensity
peaks, identical to the profile observed for the reduced E7wt
stock sample without glutathione incubation (not shown),
confirming its reduced condition. The incubation of E7wt in mild
oxidative conditions (N :1) at 8 °C led to a decrease in the
intensity of peak 6 and to the appearance of four additional peaks
in the RP-HPLC chromatogram (Figure 2B, middle panel). The
most intense peak (peak 1) showed a retention time of ~27 min.
The treatment of E7wt with 0.15 mM H₂O₂ at 37 °C for 30 min
led to protein oxidation and to the appearance of 5 additional
peaks (Figure 2B, bottom panel). The most intense peak
observed in the peroxide-oxidized E7 chromatogram (peak 1)
also showed a retention time of ~27 min, identical within
experimental error to that observed using glutathione.

Although both glutathione and H₂O₂ are considered as generic
oxidants, the mechanism and nature of the chemical modification
produced in proteins can differ. Glutathione is a rather specific
oxidant and can form mixed disulfides with protein cysteines (S-
glutathionylation) or promote the formation of intra- or
intermolecular disulfide bridges. On the other hand, H₂O₂ is
less specific and can oxidize cysteine to sulfenic, sulfinic, and
sulfonic acid, as well as other side chain groups including
methionine, tyrosine, histidine, and tryptophan.⁵² Despite the
mechanistic and chemical differences between both oxidants, the
chromatographic profiles obtained after oxidation was very
similar (i.e., the same number and retention time for each peak)
(Figure 2B), suggesting that the oxidized products were
comparable. The higher specificity of glutathione for studying
cysteine oxidation led us to continue experiments using this
reagent.

We further analyzed oxidation products using mass spectro-
scopy and SDS-PAGE techniques.

The glutathione-oxidized (N :1) E7wt sample containing at
least 70% of peak 1 species (Figure 2B) presented a major ion of
11166 m/z (Figure 2C). At this point we were unable to
discriminate whether this molecular mass peak corresponded to
fully reduced E7 or to an E7 monomer containing one or more
intramolecular disulfide bridges, since the expected mass
difference of 2 Da for formation of a single disulfide bridge is
below the technique resolution for this molecular mass range (10
Da, 0.1%). However, the fact that no covalent dimers or
oligomeric species were detected by MALDI-TOF suggested
that the oxidation event triggered by glutathione could

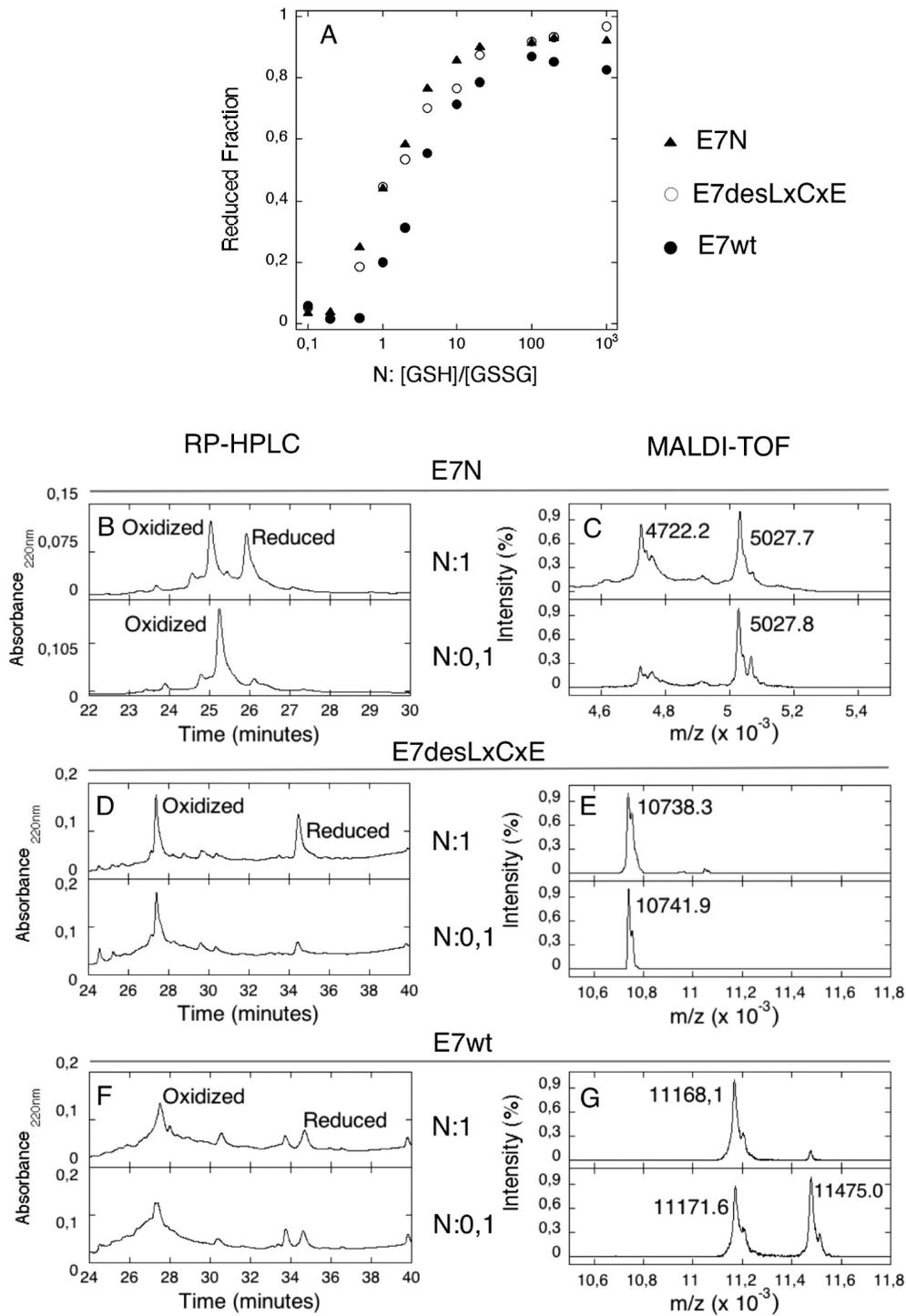


Figure 3. Assessment of redox centers in the E7 protein. (A) Redox titration of E7 variants in glutathione redox buffer. Each point corresponds to an independent sample incubated overnight at the stated [GSH]:[GSSG] *N* ratio: E7N (▲); E7desLxCxE (○); E7wt (●). (B) RP-HPLC chromatogram and (C) MALDI-TOF spectrum of E7N incubated at a ratio of *N*:1 (upper panel) or *N*:0.1 (lower panel). (D) RP-HPLC chromatogram and (E) MALDI-TOF spectrum of E7desLxCxE incubated at a ratio of *N*:1 (upper panel) or *N*:0.1 (lower panel). (F) RP-HPLC chromatogram and (G) MALDI-TOF spectrum of E7wt incubated at a ratio of *N*:1 (upper panel) or *N*:0.1 (lower panel). The chromatogram and MALDI-TOF spectrum of E7wt at a ratio of *N*:1 are the same shown in Figure 2B and are presented here for comparative purposes. Observed *m/z* values for major peaks are reported in each MALDI-TOF spectrum. Minor shifts in the retention time for the same species at the different *N* ratios are observed and can be expected due to experimental variability.

504 correspond to an intramolecular oxidation event involving
 505 cysteines or to the formation of mixed disulfides.
 506 Although a minor peak matching the molecular weight of the
 507 protein plus one glutathione molecule (307.3 Da) was observed
 508 (11475 *m/z*, Figure 2C, inset), its low intensity suggested that

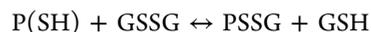
509 mixed disulfides were underrepresented in the glutathione-
 510 oxidized sample at this *N* ratio. An SDS-PAGE experiment
 511 further confirmed that oxidized E7wt was mainly monomeric, as
 512 no major differences were observed when comparing oxidized

513 and reduced E7wt samples or oxidized and reduced E7wt treated
514 with IAA to quench residual reductant equivalents (Figure 2D).

515 **Dissecting Redox Changes in the E7 Protein.** A protein
516 with seven cysteines can undergo several oxidation reactions
517 including the formation of many potential disulfide bridges
518 between either of its residues, making identification of the redox
519 center experimentally complex. To address this problem, we took
520 a fragmentation approach and first assessed the oxidative
521 behavior of the chemically synthesized 40-residue encompassing
522 the entire HPV16 E7N domain, which includes cysteine 24 from
523 the LxCxE motif (Figure 1). Additionally, we obtained an
524 HPV16 E7 mutant where amino acids LYCYE corresponding to
525 the Rb binding site (positions 21–26 of the HPV16 sequence)
526 were mutated to the SSAAA sequence. In this mutant, named
527 E7desLxCxE, all remaining cysteines are located in the globular
528 C-terminal domain (Figure 1).

529 E7wt, E7N, and E7desLxCxE were incubated overnight in
530 phosphate buffer pH 7.5 at variable glutathione *N* ratios. The
531 redox reaction was quenched by the addition of 0.1% TFA, and
532 reduced and oxidized species were resolved by RP-HPLC and
533 quantified by integration of peak areas. The E7wt protein showed
534 a redox transition with an increase in the reduced fraction as *N*
535 became higher (i.e., increase the GSH proportion) (Figure 3A).
536 We further observed that the E7N and E7desLxCxE could be
537 independently oxidized by increasing the GSSG concentration
538 (Figure 3A), although the *N* range at which the oxidation
539 reaction occurred varied for each protein. On the basis of the
540 experimental data, we can conclude that the cysteine 24 present
541 in the E7N can be readily oxidized, whereas on the other hand the
542 elimination of the cysteine 24 in the E7desLxCxE protein does
543 not preclude the oxidation of this mutant. The *N* ratio at which
544 the E7N and E7desLxCxE oxidation occurs is roughly the same.
545 Our interpretation is that in the full length protein two redox
546 centers could coexist, one at the cysteine 24 (reported by the
547 oxidation of the E7N) and the other involving one or more
548 cysteines at the C-terminal domain (reported by the oxidation of
549 the E7desLxCxE protein). However, whether these two potential
550 redox centers are independently oxidized in the E7wt protein
551 required further experimental analysis.

552 To gain information on the chemical nature of the redox
553 modification occurring in the IDD N-terminal and globular C-
554 terminal E7 domains, we further analyzed the redox curve by RP-
555 HPLC and MALDI-TOF, with representative profiles in mild
556 (*N*:1) and strong (*N*:0.1) oxidizing conditions shown in Figure
557 3B–G. E7N showed two well resolved peaks by RP-HPLC at a
558 ratio of *N*:1, with the oxidized and reduced peaks eluting at
559 roughly 25 and 26 min, respectively (Figure 3B, upper panel).
560 When this sample was analyzed by MALDI-TOF, two species
561 were identified: one with an observed molecular ion mass of $[M$
562 $+ H]^+$ of 4722.2 *m/z* corresponding to the unmodified peptide
563 (expected $[M + H]^+$ 4720.0 *m/z*) and a second assigned to a
564 mixed disulfide between the peptide and glutathione (observed
565 $[M + H]^+$ = 5027.7 *m/z*, expected $[M + H]^+$ = 5025.3 *m/z*)
566 (Figure 3C, upper panel). When E7N was incubated at a ratio of
567 *N*:0.1 (10 times more GSSG over GSH), only one peak
568 corresponding to the oxidized species was observed both in the
569 RP-HPLC chromatogram (Figure 3B bottom panel) and the
570 MALDI-TOF spectrum showed a single peak assigned to an
571 E7N-glutathione mixed disulfide (observed $[M + H]^+$ = 5027.8
572 *m/z*) (Figure 3C, bottom panel). On the basis of these results, we
573 fit the titration data to a model that considers the formation of a
574 single mixed disulfide bridge between glutathione and cysteine
575 24:



Using this model, we obtained a K_{mix} of 1.04 ± 0.09 for cysteine
24 (Supplementary Figure S2). The fact that the value obtained is
very close to the K_{mix} values reported for the formation of mixed
disulfides in free cysteine and glutathione ($K_{\text{mix}} \approx 1$),⁴¹ reflects
the solvent accessible structural environment of cysteine 24,
which is located within an intrinsically disordered domain.²³

The E7desLxCxE protein incubated at ratio of *N*:1 showed
two well resolved peaks at roughly ~27 and ~34.6 min
corresponding to similar amounts of the oxidized and reduced
species, respectively (Figure 3D, upper panel). However,
MALDI-TOF analysis identified one major molecular ion of
10738.3 *m/z* and only trace amounts of mixed disulfide
(Figure 3E, upper panel). The observed signal ($[M + H]^+$ = 10738.3
m/z) could correspond either to fully reduced ($[M + H]^+$ = 10738.9
m/z) or to oxidized protein containing one internal disulfide ($[M$
 $+ H]^+$ = 10736.9) within experimental error, since the 2 Da mass
loss produced by the formation of an internal disulfide is beyond
the resolution of the technique at high (11 KDa) molecular
weight. At *N*:0.1, E7desLxCxE presented one major RP-HPLC
peak representing over 80% of the total sample based on
quantitative analysis, with a retention time of ~27 min (Figure
3D, bottom panel). MALDI-TOF identified a single major
molecular ion of 10741.9 *m/z* (Figure 3E, bottom panel). The
fact that no mixed disulfide was observed in the fully oxidized
sample suggested that this species contained an internal disulfide
bridge, although as explained above this could not be assigned
using only this technique. Therefore, on the basis of these results
we concluded so far that an oxidation event involving cysteine
residues located in the E7 C-terminal domain takes place that
does not involve the formation of a mixed disulfide.

The chromatogram and MALDI-TOF spectrum of E7wt
incubated at a ratio of *N*:1 was previously described (Figure 2)
and is shown here for comparative purposes (Figure 3F and G,
upper panel). The chromatogram profile of E7wt incubated at a
ratio of *N*:0.1 (Figure 3F, lower panel) showed no major
differences with the data for *N*:1, except for the broadening of
peak 1 eluting at 27 min. However, as opposed to the single
species observed at *N*:1, MALDI-TOF analysis at *N*:0.1 showed
two major species, one with a molecular ion of $[M + H]^+$ =
11171.6 *m/z* corresponding to the reduced protein or to the
protein with an internal disulfide and a second molecular ion $[M$
 $+ H]^+$ = 11475.0 *m/z* corresponding to the mixed disulfide
between the E7wt protein and one glutathione molecule (Figure
3G, lower panel).

This set of data can be interpreted by proposing that E7 can
suffer two distinct redox modifications. The first corresponds to
the formation of an intramolecular disulfide bridge involving
cysteine residues located in the globular C-terminal domain,
which produces a strong retention time shift of the full-length
protein by RP-HPLC (~7.6 min, from 34.6 to 27 min). Second,
we propose the formation at higher *N* ratio of a stable mixed
disulfide bridge involving cysteine 24 located in E7N. This
oxidation event does not produce a retention time shift in RP-
HPLC, which could be explained by the highly hydrophilic
nature of the N-terminal domain where the mixed disulfide
occurs. However, this oxidation event may be responsible for the
broadening of peak 1 at 27 min corresponding to oxidized E7wt,
a conclusion supported by the fact that this broadening is not
observed in oxidized E7desLxCxE, which lacks cysteine 24. The
absence of cysteine 24 in E7desLxCxE prevents mixed-disulfide
formation, coincident with the fact that this modification was not

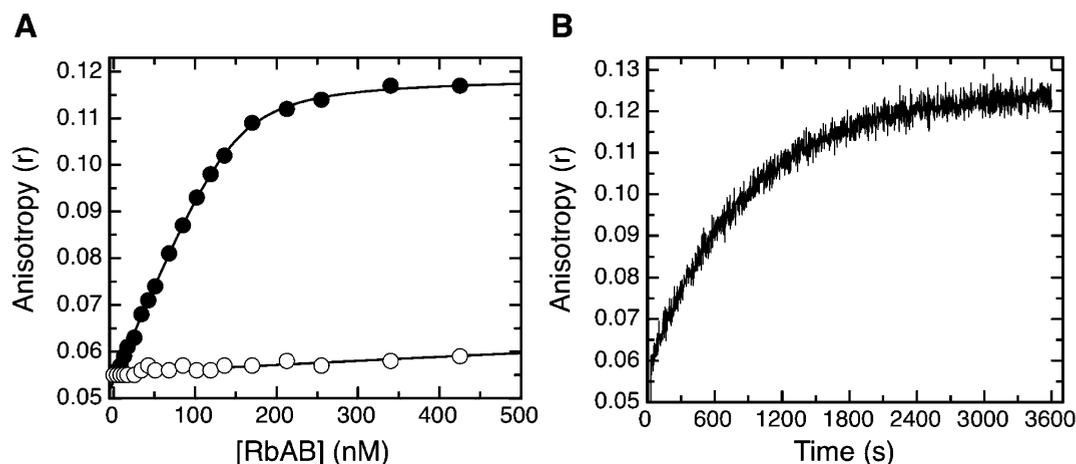


Figure 4. Binding properties of reduced and glutathionylated E7N to the RbAB domain. (A) Binding curve for the reduced (●) and glutathione-oxidized (○) E7N domain (E71-40) to the RbAB domain. The different peptides were FITC-labeled, and anisotropy at 520 nm was measured. E7N concentration was 100 nM. The affinities calculated by curve fitting were $K_D = 8.6 \pm 1.0$ nM for reduced E7N and $K_D > 6.8 \pm 0.9$ μ M for oxidized E7N. (B) Recovery of RbAB binding of oxidized E7N upon reduction with DTT. For reduction, 5 mM DTT was added to the cuvette at the end point of the titration shown in panel A (time zero). After this, fluorescence anisotropy was followed over time, showing an increase from levels characteristic of no binding ($r = 0.06$), to levels corresponding to E7N being fully reduced and bound to RbAB ($r = 0.124$).

637 observed in samples oxidized at a ratio of N:0.1 (Figure 3E, lower
638 panel). The hydrophilic nature of the E7N domain may also
639 explain why the mutation of residues 21–26 in the E7desLxCxE
640 protein has no major impact on the overall reverse-phase binding
641 behavior and retention time of the reduced and oxidized species
642 in comparison to the E7wt protein.

643 Interestingly, a different behavior of E7N and the E7wt protein
644 with respect to the formation of a mixed disulfide bridge
645 involving cysteine 24 should be noted. While E7N is fully
646 glutathionylated at a ratio of N:0.1 (Figure 3C, lower panel), the
647 E7wt protein is only partially glutathionylated at the same N ratio
648 (Figure 3G, lower panel), indicating that cysteine 24 is partially
649 protected from oxidation when found in the context of the full
650 length protein.

651 **Binding of Reduced and Oxidized E7N Species to the**
652 **RbAB Domain.** The finding that Cys 24, central to the Rb-
653 binding LxCxE motif, could be readily glutathionylated
654 prompted us to investigate the binding properties of the oxidized
655 E7N domain. For this purpose, we performed equilibrium
656 binding experiments, where we tested binding of the reduced and
657 oxidized FITC-labeled E7N domain. RbAB binding of reduced
658 E7N was measured in buffer containing 2 mM DTT, and we
659 obtained a K_D value of 8.6 ± 1.0 nM (Figure 4A) and
660 fluorescence anisotropy values of free and bound peptide of
661 0.054 and 0.12 respectively, in very good agreement with
662 previously reported values.⁴⁵ In contrast, binding of the oxidized
663 E7N peptide to RbAB was negligible with a final anisotropy value
664 at the end point of the titration of only 0.06, close to the value of
665 free peptide, and a 1000-fold reduction in binding affinity to a K_D
666 value of 6.8 ± 0.9 μ M (Figure 4A). In order to test whether this
667 drop in binding affinity depended on oxidation of Cys 24 within
668 the LxCxE motif, we added 5 mM DTT to the reaction mixture at
669 the end point of the titration, containing 100 nM oxidized FITC-
670 E7N and 1 μ M RbAB, concentrations that led to full binding of
671 the reduced peptide (Figure 4A). As can be observed, DTT
672 addition led to a slow increase in the anisotropy from a value of
673 0.06 to a final value of 0.124, characteristic of fully bound peptide
674 (Figure 4B), indicating that glutathionylation of Cys 24 was a
675 reversible process, and that Rb-binding affinity was restored
676 upon Cys 24 reduction. As binding of E7N to RbAB has been

677 shown to be a very fast process occurring in the millisecond time
678 scale ($k_{on} = 2.5 \times 10^7$ $M^{-1} s^{-1}$),⁵³ the slow increase in anisotropy
679 value reflects a slow kinetics of reduction of the mixed disulfide
680 upon DTT addition.

681 **Mapping Cysteine Connectivity in Oxidized E7.** Since
682 MALDI-TOF analysis of full length E7wt did not allow
683 characterization of intramolecular disulfide bridges, further
684 characterization of oxidized species was performed using a
685 fragmentation approach. As opposed to the direct identification
686 of the chemical species of the redox change that occurs in the
687 single cysteine contained within E7N, determination of the
688 cysteine connectivity in the C-terminal domain (containing six
689 cysteines) was a complex task that required thiol alkylation
690 followed by protein proteolysis and subsequent MALDI-TOF
691 analysis.⁵⁴ This strategy allows discrimination of cysteines that
692 are in their thiol-reduced state, which are readily alkylated with
693 iodoacetamide (IAA), from cysteines that are forming a disulfide
694 bridge and are therefore not reactive. Cysteines involved in
695 disulfide bridge formation can be further identified through the
696 direct observation of disulfide-linked peptides. We evaluated
697 cysteine connectivity using the oxidized E7desLxCxE protein,
698 which was highly enriched in the peak 1 species (>80% peak area,
699 Figure 3D) observed in both glutathione and peroxide oxidized
700 samples (Figure 2B). To this end, we prepared an oxidized
701 E7desLxCxE sample highly enriched in peak 1 species as
702 described in materials and method.

703 Although ~80% of E7desLxCxE protein is oxidized and
704 present in peak 1 at N:0.1, a residual amount of reduced protein
705 can account for low intensity fully reduced peptides that could be
706 observed in the MALDI-TOF experiment. E7 HPV16 is an acidic
707 protein with only four R or K residues, which constitute targets
708 for trypsin cleavage and are distributed over the E7 sequence
709 yielding five digestion peptides (T1–T5) that allow character-
710 ization of most of the cysteine residues within E7 (Figure 5A).
711 Three different representative samples were analyzed by
712 MALDI-TOF: (i) oxidized E7desLxCxE protein treated with
713 IAA and cleaved with trypsin; (ii) oxidized E7desLxCxE protein
714 that was treated with IAA, reduced with DTT, and cleaved with
715 trypsin; and (iii) a control stock sample of reduced E7desLxCxE
716 protein that was treated with IAA and cleaved with trypsin. The

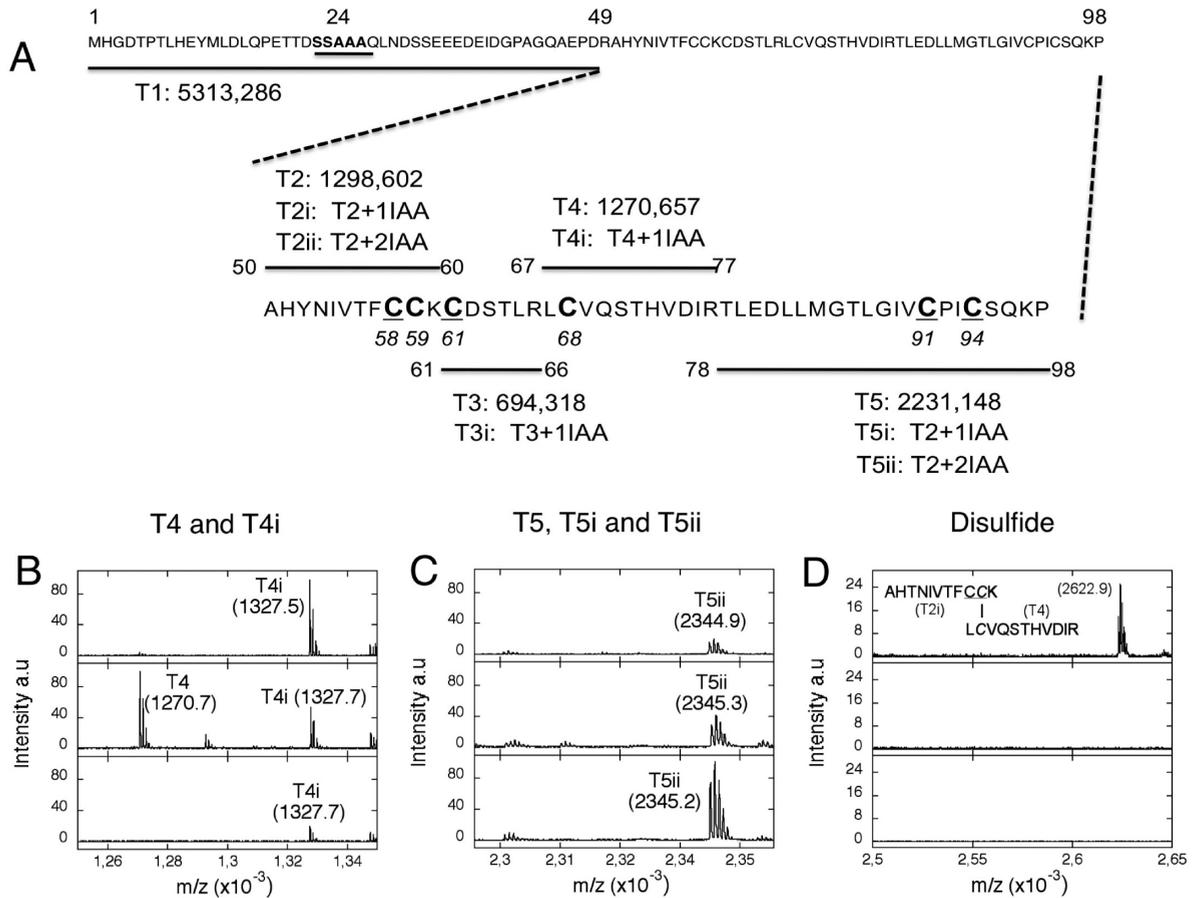


Figure 5. Identification of a disulfide bridge in oxidized E7desLxCxE. (A) Schematic representation of peptide fragments digestion expected after trypsin proteolysis of E7desLxCxE. Fragments are named by the letter T followed by a number that indicates the order of appearance in the primary sequence. All fragments contain cysteines that can be derivatized with IAA; the number of alkylated cysteines present in each fragment is indicated by the lower case letter i. Cysteines 58, 61, 91, and 94 involved in Zn binding are underlined and in bold, while noncanonical cysteines 59 and 68 are in bold. The region mutated in E7desLxCxE encompassing the Rb binding site in E7N (see fragment T1) is underlined and in bold. (B) MALDI-TOF spectra showing the T4 family ion. (C) MALDI-TOF spectra showing the T5 family ion. (D) MALDI-TOF spectra showing the disulfide-bound fragment of 2623.2 *m/z*. A schematic representation of the T2i and T4 fragments linked by a disulfide bridge is presented in the upper panel. Since the T2 fragment contains two cysteine residues (Cys 58 and 59) that are able to form a disulfide bridge, a peptide mass shift of 57 Da is observed due to the addition of one molecule of IAA. (B–D) Upper panel: oxidized E7desLxCxE sample with IAA. Middle panel: oxidized E7desLxCxE reduced with DTT after IAA addition. Lower panel: reduced E7desLxCxE sample with IAA.

Table 1. MALDI-TOF Identification of the IAA-Alkylated Fragments Obtained by the Treatment of E7desLxCxE Samples with Trypsin

fragment	expected monoisotopic (M + H) ⁺	cysteine no.	IAA	oxidized E7desLxCxE ^a	oxidized E7desLxCxE + DTT ^a	reduced E7desLxCxE ^a
T2	1298.6	58–59	0	nd	nd	nd
T2i	1355.6	58–59	1	nd	nd	nd
T2ii	1412.6	58–59	2	li	nd	li
T3	694.3	61	0	nd	nd	nd
T3i	751.3	61	1	751.2	751.3	751.3
T4	1270.7	68	0	li	1270.7	nd
T4i	1327.7	68	1	1327.5	1327.7	1327.7
T5	2231.1	91–94	0	nd	li	nd
T5i	2288.3	91–94	1	nd	li	nd
T5ii	2345.2	91–94	2	2344.9	2345,3	2345.2
T4-s-s-T2i	2623.3	58–59 and 68	1	2622.9	nd	nd

^and, not detected; li, low intensity, less than 10% of the most intense fragment.

717 results from one representative experiment are shown in Table 1.
 718 For each peptide, a series corresponding to the degree of
 719 alkylation with IAA is reported (Figure 5A and Table 1). We
 720 classified the observed ions in three main groups according to

their intensity: not detected ions (nd), ions detected at low (less
 721 than 10%) intensity (li), and ions detected at high intensity for
 722 which the observed *m/z* is shown in Table 1. Peptide T1 with an
 723 estimated molecular weight of 5313.3 Da (Figure 5A) 724

725 corresponding to the first 49 amino acids of E7desLxCxE does
726 not contain cysteine and was excluded from the analysis.

727 The T2, T2i, and T2ii peptide family containing cysteines 58
728 and 59 modified with none, one, or two IAA moieties constitutes
729 a peptide family that was poorly detected or not detected in all
730 samples including the control reduced E7desLxCxE protein.
731 Among the peptides that contain cysteine 61 (T3 and T3i) only
732 the alkylated peptide T3i was detected with high intensity in all
733 samples, indicating that cysteine 61 is reduced in the oxidized
734 E7desLxCxE protein. The peptide family containing cysteine 68
735 (T4 and T4i) showed a clear differential pattern in the oxidized
736 and the reductant-treated oxidized sample. In oxidized
737 E7desLxCxE, only the alkylated T4i peptide was detected,
738 suggesting the presence of a residual population of cysteine in a
739 reduced state. In the oxidized E7desLxCxE sample treated with
740 DTT, both peptides were clearly detected (Table 1 and Figure
741 5B). In this last sample, the intensity of the T4 ion was higher
742 than the T4i ion, suggesting that two protein populations coexist
743 in the oxidized sample, one with cysteine 68 in its reduced form
744 (yielding the T4i peptide) and the other with cysteine 68 forming
745 a disulfide bridge and therefore not reactive toward IAA (yielding
746 the T4 peptide). In the reduced sample only the alkylated T4i
747 peptide was detected. The peptide family containing cysteines 91
748 and 94 (T5, T5i, and T5ii) did not show a differential pattern
749 between the three samples, and T5ii was the only species
750 detected (Table 1 and Figure 5C), indicating that cysteines 91
751 and 94 are not forming a disulfide bridge in oxidized
752 E7desLxCxE.

753 A strong positive evidence supporting the existence of a
754 disulfide bridge was the systematic detection of a peptide of $[M +$
755 $H]^+ = 2623.3 m/z$ in the oxidized E7desLxCxE sample that was
756 assigned to a fragment containing peptides T4 (cysteine 68) and
757 T2i (cysteines 58 and 59) linked by a disulfide bridge (Table 1
758 and Figure 5D, upper panel). This fragment was not observed
759 either in the oxidized E7desLxCxE sample treated with DTT or
760 in the reduced E7desLxCxE stock sample (Figure 5D, middle
761 and lower panel). In order to confirm this result, cysteine
762 connectivity was further analyzed using *N*-ethylmaleimide
763 (NEM) as a thiol-modifying agent. The second order rate
764 constant for the reaction of an average thiol with IAA (pH \approx 8)
765 was $4.6 M^{-1} s^{-1}$, while NEM reacted 200-fold faster with a
766 constant of $10000 M^{-1} s^{-1}$.⁴¹ This large difference in reactivity
767 toward thiols can be useful to prevent rapid disulfide reshuffling
768 that can occur during sample handling.

769 The results for the NEM experiments are shown in
770 Supplementary Figure S3 and tabulated in Supplementary
771 Table 1. The results obtained with NEM fully support those
772 shown for IAA, with the same observed patterns of ions
773 compared to the IAA experiment. The TN2 ion family was
774 poorly detected as isolated fragments. Only TN3i was detected,
775 indicating that cysteine 61 was in its reduced form in the three
776 samples. The TN4 and TN4i peptides showed a clear differential
777 pattern in the oxidized and the oxidized plus DTT sample, with
778 the intensity of the TN4 ion being higher than the T4i ion in the
779 oxidized E7desLxCxE sample treated with DTT, indicating a
780 partial oxidation of cysteine 68 (Supplementary Figure S3).
781 Cysteines 91 and 93 were found in their reduced state and
782 reacted with NEM, yielding mainly the TN5ii (Supplementary
783 Figure S3). Finally, an ion of $[M + H]^+ = 2691.2 m/z$ was
784 observed in the oxidized sample only and could be assigned to a
785 fragment containing the TN4 and TN2i peptides linked by a
786 disulfide bridge (Supplementary Figure S3). Note that the
787 difference in the molecular weight of the disulfide-linked

fragment obtained in the NEM experiment versus the IAA 788
experiment is due to the differences in the molecular weight of 789
both reagents (IAA = 57 Da vs NEM = 125 Da). Taken together, 790
these data indicate that peak 1 corresponds to an oxidized species 791
containing an internal disulfide bridge between cysteine 68 and 792
either cysteine 58 or 59. Since both cysteines 58 and 59 are 793
contained within the same tryptic peptide (T2 peptide family), 794
this approach did not allow discriminating which cysteine was 795
involved in the disulfide bridge. Remarkably, three of the four 796
cysteine residues involved in Zn coordination (C61, C91, and 797
C94) were protected from oxidation, suggesting that C58 may 798
also be protected from oxidation and encounter a structural role 799
in oxidized E7. 800

Effect of C59A Mutation on E7 Redox Behavior. In order 801
to test whether cysteine 58 or 59 was the residue involved in the 802
disulfide bridge with cysteine 68, we obtained the E7C59A 803
mutant, which does not alter Zn-binding cysteines (Figure 1). 804
The C59A mutation had no effect on Zn coordination or on 805
protein stability as judged by PMPS-PAR and circular dichroism 806
(CD) measurements (not shown). The formation of the 807
disulfide-oxidized species in the E7C59A was evaluated by the 808
appearance of peak 1 by RP-HPLC following incubation with 809
different glutathione *N* ratios. 810

A first inspection of the RP-HPLC profiles in highly reducing 811
conditions (i.e., $N \geq 200$) showed important differences between 812
E7C59A and E7wt, with a marked increase in the content of 813
oxidized species in the E7C59A, detected as increments in several 814
peaks, including peak 2 and peak 4 areas (Figure 6A, upper and 815
middle panel). The chromatogram of oxidized E7C59A at 816
glutathione ratios of *N*:1 and *N*:0.1 was devoid of peak 1 817
observed in E7wt, indicating that formation of the oxidized 818
species corresponding to peak 1 requires the presence of cysteine 819
59 (Figure 6B and C, upper and middle panel). This result 820
allowed us to assign a C59–C68 connectivity for the disulfide 821
bridge identified in oxidized E7. 822

The high level of oxidation observed in reducing conditions 823
upon mutation of C59 suggested that this residue had a 824
protective effect on the overall redox state of E7 cysteines. To 825
further analyze this possibility, we tested oxidation in the 826
E7C59A-desLxCxE mutant, where cysteines 59 and 24 have been 827
replaced by alanine. Remarkably, this mutant presented a 828
chromatogram similar to that observed for E7wt (Figure 6A, 829
upper and lower panels). This result suggests that the presence of 830
cysteine 59 prevents oxidation events mediated by cysteine 24. 831
As expected by the absence of C59 in this mutant protein, no 832
evidence for the appearance of peak 1 representing the disulfide 833
linked species was observed upon incubation in oxidizing 834
conditions (Figure 6B and C, upper and lower panels). 835
Moreover, the fact that this mutant that retains C68 showed 836
very low overall levels of oxidized species, with the exception of 837
the nonidentified oxidized species peak X (Figure 6B and C, 838
lower panel), was an indication that C68 had low intrinsic 839
reactivity to oxidation. Taken together, these results confirmed 840
that the disulfide bridge in oxidized E7 involves residues C59 and 841
C68 and also indicated that the presence of cysteine 59 in the 842
wild type protein prevents the formation of oxidized E7 species in 843
reducing environments. 844

C59–C68 Disulfide Yields a Conformational Rearrangement in E7. Our experimental results indicated that the 845
disulfide bridge in oxidized E7 forms between cysteines 59 and 846
68 and does not involve the Zn-coordinating cysteines (positions 847
58, 61, 91, and 94), implying that the oxidized protein is 848
potentially able to bind the metal atom. We assessed the binding 849
850 851 852 853 854 855 856 857 858 859 860 861 862 863 864 865 866 867 868 869 870 871 872 873 874 875 876 877 878 879 880 881 882 883 884 885 886 887 888 889 890 891 892 893 894 895 896 897 898 899 900 901 902 903 904 905 906 907 908 909 910 911 912 913 914 915 916 917 918 919 920 921 922 923 924 925 926 927 928 929 930 931 932 933 934 935 936 937 938 939 940 941 942 943 944 945 946 947 948 949 950 951 952 953 954 955 956 957 958 959 960 961 962 963 964 965 966 967 968 969 970 971 972 973 974 975 976 977 978 979 980 981 982 983 984 985 986 987 988 989 990 991 992 993 994 995 996 997 998 999 1000

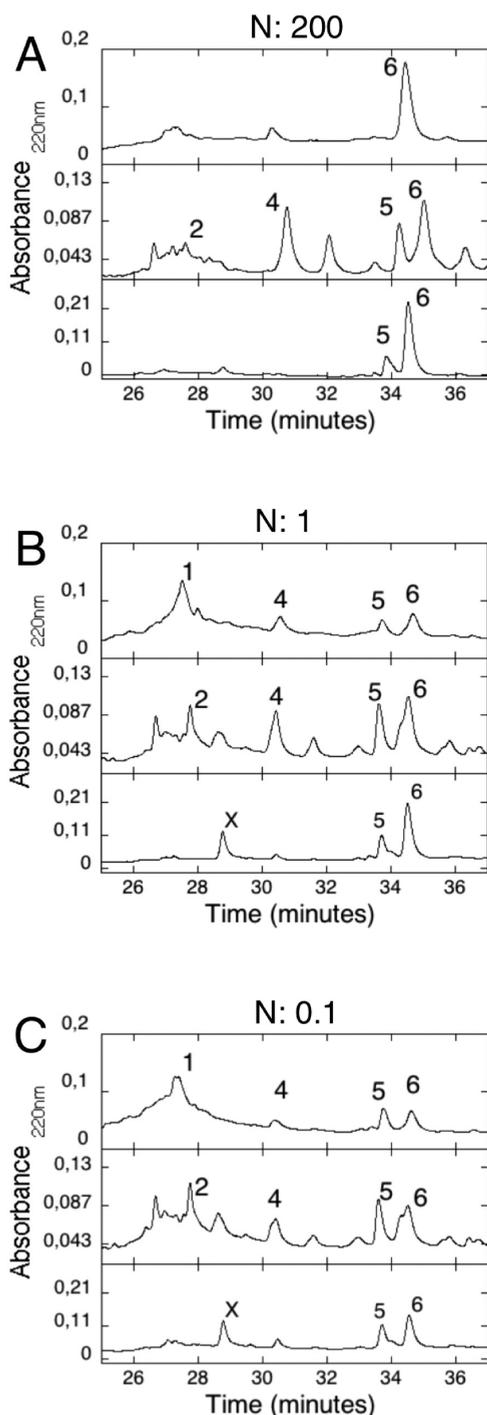


Figure 6. Effect of mutation of C59 and C59/C24 on E7 redox behavior. (A) RP-HPLC chromatogram of E7wt (upper panel), E7C59A (middle panel), and E7C59A-desLxCxE (lower panel) samples incubated with glutathione at a ratio of $N:200$ (highly reducing conditions). (B) RP-HPLC chromatogram of E7wt (upper panel), E7C59A (middle panel), and E7C59A-desLxCxE (lower panel) samples incubated with glutathione at a ratio of $N:1$. (C) RP-HPLC chromatogram of E7wt (upper panel), E7C59A (middle panel), and E7C59A-desLxCxE (lower panel) samples incubated with glutathione at a ratio of $N:0.1$ (highly oxidizing conditions). Peak numbering is as in Figure 2, with peak 6 corresponding to the fully reduced protein. Peak "X" appears only in E7C59A-desLxCxE oxidized samples.

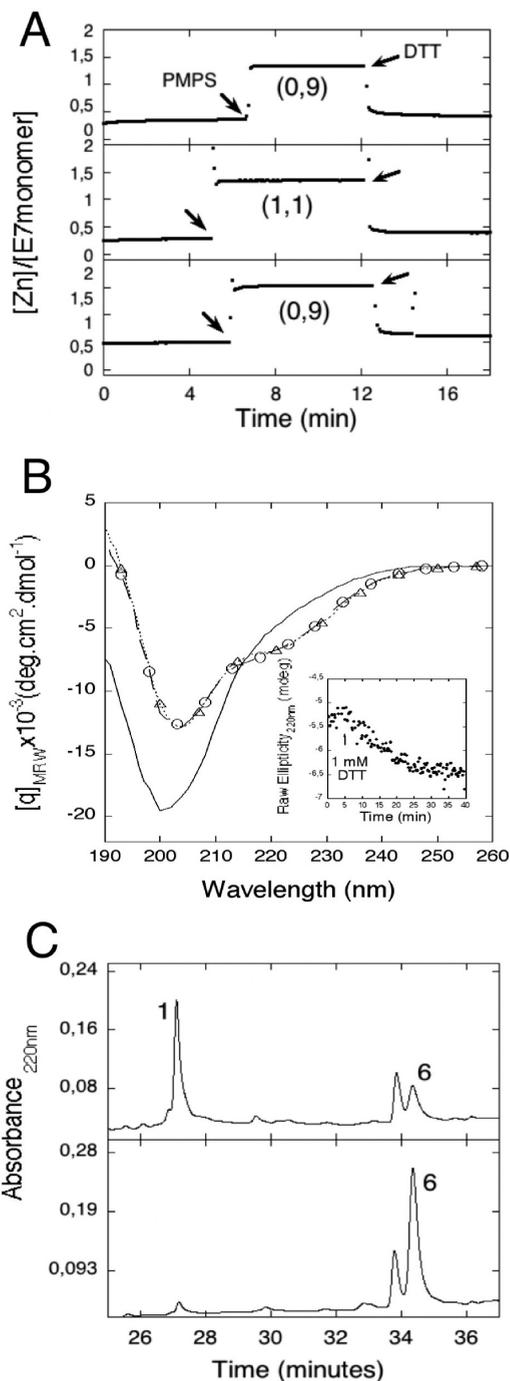


Figure 7. Metal binding and conformation of oxidized E7desLxCxE. (A) Quantitative evaluation of strongly bound Zn in oxidized E7desLxCxE (upper panel), reduced E7desLxCxE (middle panel), and reduced E7wt (lower panel). The addition of $100 \mu\text{M}$ PMPS is indicated by an arrow. Released Zn was quantified by a colorimetric reaction with PAR (see Materials and Methods). Cysteines were unblocked by the addition of $250 \mu\text{M}$ DTT, indicated by a second arrow. (B) Far-UV CD spectra of reduced E7desLxCxE (dotted line with triangles), oxidized E7desLxCxE (full line), and oxidized E7desLxCxE that had been reduced by incubating the protein for 1 h at 37°C with 1 mM DTT (full line with circles). Inset: kinetics of reduction of oxidized E7desLxCxE followed by molar ellipticity at 220 nm, initiated by adding 1 mM of DTT at 37°C (indicated by an arrow). (C) RP-HPLC chromatogram of oxidized E7desLxCxE before (upper panel) and after reduction with DTT (lower panel).

851 properties of oxidized E7desLxCxE (Figure 7A, upper panel),
852 reduced E7desLxCxE (Figure 7A, middle panel), and reduced

853 E7wt protein (Figure 7A, lower panel) using the colorimetric
854 detection of PAR-Zn complexes.⁴³ Surprisingly, all three samples
855 showed a ~1:1 Zn:protein stoichiometry, indicating that
856 oxidized E7desLxCxE was able to bind Zn despite the formation
857 of a disulfide bridge between cysteines 59 and 68. We assessed
858 the relative affinity for the Zn-protein interaction by comparing
859 the ability of PAR to compete for the protein-bound metal. The
860 PAR-Zn complex has a reported equilibrium constant K_d of
861 $\sim 10^{-12}$ M,⁴³ and the estimated dissociation constant for the
862 E7wt-Zn complex was lower, since 100 μ M concentration of
863 PAR present in the sample was unable to displace high affinity
864 protein-bound Zn (Figure 7A). The addition of PMPS produced
865 the release of Zn, which in turn formed a colored complex with
866 PAR producing an abrupt increase of the absorbance at 500 nm
867 (Figure 6A). The subsequent addition of DTT released PMPS-
868 blocked cysteines, leading to Zn reuptake by the protein and to a
869 decrease in the absorbance at 500 nm.⁴³ Oxidized E7desLxCxE
870 showed a behavior similar to that observed for reduced
871 E7desLxCxE and E7wt, suggesting that oxidized E7desLxCxE
872 maintains its high affinity Zn-binding site and that the oxidized
873 protein is able to reuptake the metal ion once its cysteines have
874 been released from PMPS (Figure 7A). The protein samples
875 contain a basal, substoichiometric amount of spurious metal
876 detected by the level of the basal absorbance at 500 nm that
877 corresponds to soft-bound metal, not necessarily Zn, which is
878 readily complexed by PAR without the addition of PMPS.

879 According to the published structures of E7 from the HPV1A
880 and HPV45 types,^{21,22} cysteines 59 and 68 in HPV16 E7 would
881 be located too distant from each other (18.6 Å) to be able to form
882 a disulfide bridge without the protein suffering a considerable
883 rearrangement in its secondary and tertiary structure (Figure
884 1C). To assess this point, we performed far-UV CD measure-
885 ments of reduced and oxidized E7desLxCxE (Figure 7B). As a
886 control, we compared the CD spectrum of reduced E7desLxCxE
887 to that of reduced E7wt, which has been thoroughly
888 characterized,²⁰ observing no significant differences among
889 them (not shown). The CD spectrum of oxidized E7desLxCxE
890 differed clearly from that of reduced E7desLxCxE (Figure 6B),
891 presenting a decrease in the absolute value of the negative
892 shoulder at 220 nm, assigned to an α -helical structure present in
893 the native E7 structure (Figure 1), as well as an increase in the
894 absolute value of the negative band at 200 nm that has been
895 assigned to intrinsically disordered elements, likely at the E7N
896 IDD.^{20,23} Together, these results indicated that oxidized
897 E7desLxCxE presented a loss of canonical secondary structure
898 elements. Despite the changes observed in the protein secondary
899 structure, oxidized E7 preserved its ability to bind Zn and
900 reuptake it with high affinity (Figure 7A). Finally, the addition of
901 1 mM DTT led to a slow reversal of these structural changes
902 (Figure 7B, inset), yielding a final CD spectrum that could be
903 superimposed to that of the reduced protein (Figure 7B). The
904 reversibility of the oxidation process was also verified by RP-
905 HPLC, where addition of 5 mM DTT to an oxidized
906 E7desLxCxE sample led to full recovery of the reduced peak 6
907 (Figure 7C).

908 ■ DISCUSSION

909 E7 is a small oncoprotein that plays a crucial role in the HPV virus
910 life cycle and in cervical cancer development in humans.⁹
911 Considerable work has been conducted to understand its
912 functional and structural properties; however, despite the fact
913 that HPV16 E7 shows high cysteine content and that 12 out of
914 the 13 high risk HPV E7 proteins contain at least two

noncanonical cysteines, its redox behavior has not been 915
investigated to date. In the present work we show the effect of 916
oxidative conditions on E7, we describe two distinct redox 917
centers in the HPV16 E7 oncoprotein involving cysteine 24 and 918
the cysteine 59/68 pair, respectively, and we demonstrate the 919
protective effect of noncanonical cysteine 59 on the overall E7 920
redox state. 921

Strictly conserved cysteines involved in Zn binding have been 922
widely studied, revealing a marked decrease in protein stability 923
upon mutation,^{55,56} and cysteine 24 within the LxCxE motif was 924
pointed out as an important residue for Rb binding.⁵⁷ The fact 925
that noncanonical cysteines 59 and 68 in HPV16 E7 do not show 926
strict conservation across papillomavirus E7 proteins may be the 927
reason why this cysteine pair has not been previously identified as 928
a potential site of redox regulation of E7 proteins. 929

Our study shows that despite its high cysteine content all seven 930
cysteine residues within HPV16 E7 are in their reduced state 931
under conditions that resemble the basal reducing environment 932
of the cell cytoplasm.⁵⁰ However, E7 undergoes a controlled 933
oxidation process upon the addition of biologically compatible 934
oxidants such as hydrogen peroxide (H_2O_2) and glutathione 935
(GSSG) (Figure 2). One redox center in E7 involves the solvent- 936
exposed cysteine 24 located within the LXCXE Rb binding motif 937
in the intrinsically disordered N-terminal domain of E7. This 938
cysteine is readily glutathionylated in the context of the isolated 939
E7N domain and has a K_{mix} value close to 1, similar to that 940
observed for free alkyl thiols.⁴¹ The fact that this residue is within 941
a disordered domain and exposed to the solvent indicates that it 942
could be easily oxidized (i.e., undergo redox regulation) under 943
stress conditions. Moreover, we demonstrate that Cys 24 944
glutathionylation abolishes Rb-binding, a process that is fully 945
reversible by the addition of DTT and leads to full recovery of 946
Rb-binding (Figure 4). A second redox center is located in the E7 947
C-terminal domain, where we show the formation of an internal 948
disulfide bridge between cysteines 59 and 68 through peptide 949
mapping (Figure 5). However, our results show that in the 950
context of the full-length protein cysteine 24 is protected from 951
oxidation and less prone to glutathionylation than in the context 952
of the isolated E7N peptide (Figure 3), indicating that the C- 953
terminal cysteine-rich domain can prevent the glutathione- 954
induced oxidation of cysteine 24. The protective effect of the 955
E7C domain over the E7N domain strongly suggests an 956
unexpected long-range interdomain interaction. 957

The fact that two very different oxidative agents lead to the 958
same oxidized E7 end-product (peak 1) recalls canalization, an 959
evolutionary process whereby a population produces similar 960
phenotypes regardless of environmental variability,⁵⁸ and 961
suggests the presence of a common and evolved oxidation 962
mechanism. Moreover, oxidation of solvent-accessible cysteine 963
24 is diminished in the context of the E7wt protein (Figure 3), 964
and removal of cysteine 59 leads to loss of peak 1 (C59–C58 965
disulfide bridge) and to an increase in basal-state oxidation in 966
conditions ($N > 200$) where the wild type protein remains fully 967
reduced, suggesting that the evolutionary conservation of 968
noncanonical cysteines in the E7 sequence is functionally driven. 969
Considering the fact that the E7 oncoprotein performs its 970
functions in an oxidative environment,^{16,17,19} a likely hypothesis 971
is that noncanonical cysteines protect the E7 protein against 972
oxidative damage and consequent loss of function as suggested 973
by our experimental results (Figure 4). Alternatively, C24 974
oxidation could serve as a sensor for redox regulation of Rb 975
binding, modulating the interaction affinity. 976

977 Analysis of surface accessibility of the positions corresponding
 978 to residues C59 and C68 in HPV16 E7 reveals that while cysteine
 979 S9 is highly exposed in both the dimeric and monomeric E7
 980 structures (Figure 8 and Table 2), the position corresponding to

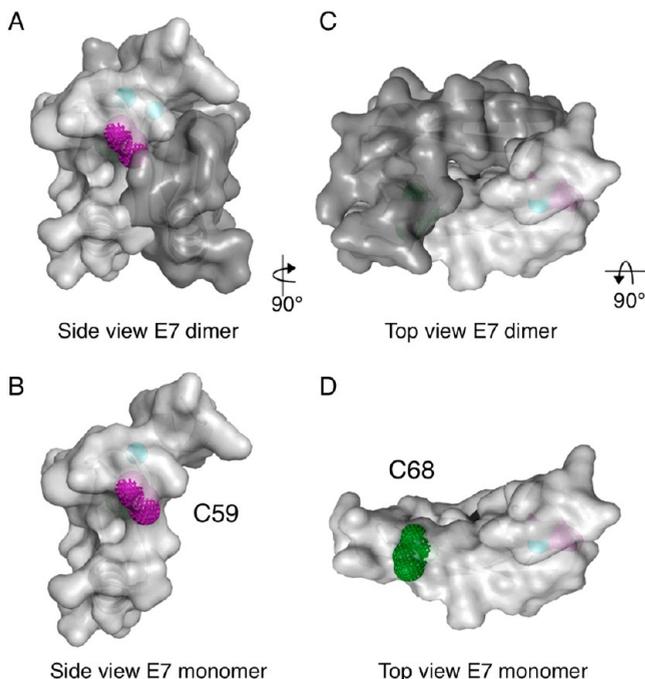


Figure 8. Changes in exposure of noncanonical cysteines in E7 upon dimer dissociation. (A, B) Side view of HPV16 E7 dimer modeled showing the changes in exposure of cysteine 59 (pink) upon dissociation of the E7 dimer. (C, D) Top view of the HPV16 E7 dimer showing the changes in exposure of cysteine 68 (green) upon dissociation of the E7 dimer. The HPV16 E7 dimer was modeled using Modeler and the HPV45 E7 dimer structure (PDB id: 2F8B) as a template, with both E7 monomers depicted in light and dark gray, respectively. The rotation of structures with respect to the orientation depicted in Figure 1B is indicated.

981 cysteine 68 (threonine in HPV45 E7) is fully buried in the dimer
 982 interface but becomes exposed upon dimer dissociation (Figure
 983 8 and Table 2). Moreover, we have experimentally demonstrated
 984 that the E7 oxidation shows a marked dependence with the total
 985 protein concentration (Supplementary Figure S4), indicating
 986 that a dimer to monomer equilibrium shift led to an increase of
 987 the amount of the oxidized E7 species (peak 1). Altogether, this
 988 evidence suggests that the formation of the C59–C68 disulfide
 989 requires E7 dimer dissociation. The low amount of oxidized
 990 dimeric or oligomeric species observed in this study further
 991 suggests that oxidation may proceed through a monomeric E7
 992 intermediate (Figure 2C), in line with the weak ($\sim 1 \mu\text{M}$)
 993 reported dissociation constant for the E7 dimer.²⁴

994 The distance between positions 59 and 68 within the E7
 995 HPV16 monomer is about 18.6 Å (Figure 1). This implies that
 996 the formation of a disulfide bridge between C59 and C68 must
 997 necessarily be accompanied by a large-scale rearrangement of the
 998 protein secondary and tertiary structure. Such changes are
 999 reported by the pronounced difference between the far-UV CD
 1000 spectra of the oxidized and reduced E7desLxCxE protein.
 1001 Interestingly, the conformational transition induced upon E7
 1002 oxidation is fully reversible, as indicated by restoration of the
 1003 reduced far-UV CD spectrum upon DTT addition (Figure 7B),
 1004 supporting a regulatory role of this species. The fact that the

Table 2. Relative Accessibility for Cysteine-Rich Positions 24, 59, and 68 in E7

cysteine	location	HPV45 E7 ^a dimer	HPV45 E7 ^a monomer	HPV16 E7 ^a monomer	experimental reactivity
24	canonical Rb binding			IDD	$K_{\text{mix}} = 1^d$
58	canonical Zn binding	0	0	0	nr ^e
59	noncanonical	0.62 ^b	0.63 ^b	0.47	disulfide ^e
61	canonical Zn binding	0.37	0.43	0.5	nr ^e
68	noncanonical	0.007 ^c	0.51 ^c	0.72	disulfide ^e
91	canonical Zn binding	0.09	0.16	0.06	nr ^e
94	canonical Zn binding	0.01	0.05	0.08	nr ^e

^aRelative accessibility for cysteine residues was calculated using the DSSP algorithm,⁴⁹ with exposed surface areas normalized per maximal residue area (see Materials and Methods). Cysteine residues with relative accessibility values >0.2 were considered accessible, and those with values <0.2 were considered buried. ^bThe position corresponding to Cys 59 in HPV 16 E7 is also a cysteine in HPV45 E7. ^cThe position corresponding to Cys 68 in HPV16 E7 is a threonine residue in HPV45 E7. ^dReactivity was judged by comparison of the K_{mix} value to that of free cysteine ($K_{\text{mix}} \sim 1$).⁴¹ ^eReactivity was derived from oxidation followed by MALDI-TOF analysis (Figure 4 and Table 1)

oxidized species retains strong Zn coordination despite the
 strained conformation induced by the disulfide bridge formation,
 suggests that the Zn binding motif may act as a scaffold to help
 guide the structural changes leading back to the native state upon
 reduction of the disulfide bridge. In support of this mechanism,
 experimental evidence suggests that, with few exceptions,^{59,60} Zn
 binding cysteines are less reactive to oxidation than others
 cysteines, as they are protected by metal coordination (Table
 2).⁶¹ Many proteins regulated by disulfide formation present
 cysteines that are far apart from each other in the reduced state. A
 paradigmatic example is the redox-responsive regulator OxyR, a
 transcription factor activated upon exposure to hydrogen
 peroxide.⁶² This regulator forms an intramolecular disulfide
 bridge between cysteines located 17 Å apart in the reduced
 inactive form, which is accompanied by a dramatic structural
 change in the regulatory domain.⁶³ Similarly, formation of an
 internal disulfide bridge in intracellular chloride ion channel
 proteins (CLICs) induces a major structural rearrangement and
 changes in the oligomerization state, as revealed by crystallo-
 graphic studies of the oxidized form.⁶⁴

Cysteine 59 is located in Cluster 1, proximal to the Zn binding
 site of the same monomer and is exposed in both the dimer and
 monomer structures (Figures 1 and 8A,C). Remarkably, the
 position immediately following C59 is occupied by a basic
 residue in most HPV E7 proteins (Figure 1), a feature known to
 lower cysteine pK_a, increasing its chemical reactivity.^{31,40,65}
 These structural features suggest that C59 is a highly reactive
 cysteine, thus likely to play a functional role. On the other hand,
 C68 belongs to Cluster 2 and is buried in the dimer structure,
 requiring monomerization in order to be exposed (Figure 8
 B,D). Moreover, experiments with the E7C59A-desLxCxE
 variant indicate that C68 has low propensity to oxidation (Figure
 5), suggesting that this cysteine has low reactivity. The presence
 of an exposed reactive cysteine surrounded by basic residues is a
 common mechanistic feature of proteins that are redox regulated
 due to conformational changes triggered by disulfide formation

1041 such as OxIR⁶³ as well as of proteins involved in redox catalysis
1042 such as peroxiredoxin.⁶⁶

1043 In redox regulated proteins such as OxyR, the C199 reactive
1044 cysteine has a positively charged environment and serves as the
1045 stimulus sensor, which is easily oxidized by H₂O₂, initiating a
1046 conformational change that allows for disulfide bond forma-
1047 tion.⁶³ On the other hand, the existence of a highly reactive Cys
1048 may support an effective redox catalytic cycle, a mechanism that
1049 has been well studied in atypical mammalian 2-Cys peroxiredoxin
1050 (Prdx S).^{66,67} Whether noncanonical cysteines in E7 proteins
1051 possess a relevant function, either as a conformational switch
1052 modulating the multiple target repertoire of E7 or in redox
1053 catalysis protecting C24 from oxidation in an oxidized milieu,
1054 requires further research. In both scenarios, C59 could act as the
1055 reactive or catalytic cysteine and C68 as a resolving cysteine.
1056 Reversibility is strictly required to accomplish both regulatory
1057 and catalytic functions, a condition that is fulfilled by the redox
1058 behavior of the E7 HPV16 protein (Figure 7). Additionally,
1059 sequence analysis shows that virtually all E7 proteins presenting
1060 at least two noncanonical cysteines possess one cysteine in
1061 Cluster 1, a cluster likely to harbor exposed and highly reactive
1062 cysteines.²⁵ In line with this, some peroxiredoxins (1-Cys) lack
1063 the resolving cysteine, which is substituted by low molecular
1064 weight thiols, but the absence of a catalytic cysteine is
1065 irreplaceable for redox activity.⁶⁸

1066 A possible direct function for a redox catalytic pair in E7 could
1067 involve maintaining C24 in a reduced state, allowing Rb binding
1068 despite the presence of the oxidative environment observed in
1069 HPV-transformed tissues. In support of this, our results show
1070 that the full length E7 protein partially protects C24 from
1071 glutathionylation (Figure 3). Recently, it has been reported that
1072 the Glutathione S-transferase P1 (GST-P1) protein is also a
1073 target of HPV16 E7 protein.¹⁹ E7 binds to GST-P1 through a
1074 region that comprises amino acids 40–60 of the E7 sequence,
1075 and the E7-GSTP1 interaction modifies the redox equilibrium
1076 between the reduced and oxidized GST-P1 protein in favor of the
1077 reduced state of the enzyme.¹⁹ The reduced GST-P1 interacts
1078 and inhibits the c-Jun N-terminal kinase (JNK), which in turn is
1079 unable to phosphorylate the Jun protein. Since JNK-mediated
1080 signal transduction leads to apoptosis, it has been suggested that
1081 this is the mechanism by which HPV16 E7 transformed
1082 keratinocytes escape apoptosis.

1083 The presence of noncanonical cysteines in 70% of E7
1084 sequences including most clinically relevant HPV strains suggests
1085 that redox regulation may be a common property shared by a
1086 large number of E7 proteins, and the study of redox mechanisms
1087 is of particular interest in high-risk E7 proteins, known to be
1088 constitutively expressed in an oxidative environment within
1089 HPV-transformed cells. Finally, the multiple reported cellular
1090 effects of E7 could well be related to moonlighting functions that
1091 are redox-regulated. In this scenario, redox regulation provides an
1092 additional layer of conformational diversity to E7, allowing this
1093 small multitarget viral protein to gain complexity without paying
1094 the cost of an enlarged viral genome size.

1095 ■ ASSOCIATED CONTENT

1096 ● Supporting Information

1097 Supplementary Figures S1–S4 and Supplementary Table 1. This
1098 material is available free of charge via the Internet at [http://pubs.](http://pubs.acs.org)
1099 [acs.org](http://pubs.acs.org).

1100 ■ AUTHOR INFORMATION

1101 Corresponding Authors

*Ph: +54 11 52387500. E-mail: gpg@leloir.org.ar. 1102

*Ph: +54 11 52387500. E-mail: lalonso@leloir.org.ar. 1103

1104 Author Contributions

[§]These authors contributed equally to this work. 1105

1106 Funding

This work was supported by a Grant for Basic Research from 1107
Instituto Nacional del Cáncer (National Health Ministry, 1108
Argentina). All authors are career investigators from Consejo 1109
Nacional de Investigaciones Científicas y Técnicas (CONICET, 1110
Science and Technology Ministry, Argentina). 1111

1112 Notes

The authors declare no competing financial interest. 1113

1114 ■ ABBREVIATIONS

HPV, human papillomavirus; Rb, retinoblastoma protein; IDD, 1115
intrinsically disordered domain; E7SOs, E7 spherical soluble 1116
oligomers; DTT, dithiothreitol; PMPS, *p*-hydroxymercuriphe- 1117
nylsulfonate; PAR, 4-(2-pyridylazo) resorcinol; DTNB, 5,5'- 1118
dithiobis(2-nitrobenzoic acid); GSH, reduced glutathione; 1119
GSSG, oxidized glutathione; RP-HPLC, reverse-phase high- 1120
performance liquid chromatography; IAA, iodoacetamide; NEM, 1121
N-ethylmaleimide; CD, circular dichroism; GdmCl, guanidinium 1122
chloride; TFA, trifluoroacetic acid; OPG, octyl β -D-glucopyrano- 1123
side; HCCA, α -cyano-4-hydroxycinnamic acid 1124

1125 ■ REFERENCES

- 1126 (1) zur Hausen, H. (1996) Papillomavirus infections—a major cause of 1126
human cancers. *Biochim. Biophys. Acta* 1288, F55–78. 1127
- 1128 (2) Munoz, N., Bosch, F. X., de Sanjose, S., Herrero, R., Castellsague, 1128
X., Shah, K. V., Snijders, P. J., and Meijer, C. J. (2003) Epidemiologic 1129
classification of human papillomavirus types associated with cervical 1130
cancer. *N. Engl. J. Med.* 348, 518–527. 1131
- 1132 (3) Bernard, H. U., Burk, R. D., Chen, Z., van Doorslaer, K., zur 1132
Hausen, H., and de Villiers, E. M. (2010) Classification of 1133
papillomaviruses (PVs) based on 189 PV types and proposal of 1134
taxonomic amendments. *Virology* 401, 70–79. 1135
- 1136 (4) Schiffman, M., Herrero, R., Desalle, R., Hildesheim, A., Wacholder, 1136
S., Rodriguez, A. C., Bratti, M. C., Sherman, M. E., Morales, J., Guillen, 1137
D., Alfaro, M., Hutchinson, M., Wright, T. C., Solomon, D., Chen, Z., 1138
Schussler, J., Castle, P. E., and Burk, R. D. (2005) The carcinogenicity of 1139
human papillomavirus types reflects viral evolution. *Virology* 337, 76– 1140
84. 1141
- 1142 (5) Doorbar, J. (2005) The papillomavirus life cycle. *J. Clin. Virol.* 32 1142
(Suppl 1), S7–15. 1143
- 1144 (6) Howley, P. M. (1996) *Fields Virology*, 3rd ed., Raven Publishers, 1144
Philadelphia. 1145
- 1146 (7) Helt, A. M., Funk, J. O., and Galloway, D. A. (2002) Inactivation of 1146
both the retinoblastoma tumor suppressor and p21 by the human 1147
papillomavirus type 16 E7 oncoprotein is necessary to inhibit cell cycle 1148
arrest in human epithelial cells. *J. Virol.* 76, 10559–10568. 1149
- 1150 (8) Banerjee, N. S., Genovese, N. J., Noya, F., Chien, W. M., Broker, T. 1150
R., and Chow, L. T. (2006) Conditionally activated E7 proteins of high- 1151
risk and low-risk human papillomaviruses induce S phase in postmitotic, 1152
differentiated human keratinocytes. *J. Virol.* 80, 6517–6524. 1153
- 1154 (9) Moody, C. A., and Laimins, L. A. (2010) Human papillomavirus 1154
oncoproteins: pathways to transformation. *Nat. Rev. Cancer* 10, 550– 1155
560. 1156
- 1157 (10) Pim, D., and Banks, L. (2010) Interaction of viral oncoproteins 1157
with cellular target molecules: infection with high-risk vs low-risk human 1158
papillomaviruses. *APMIS* 118, 471–493. 1159
- 1160 (11) Dyson, N., Howley, P. M., Munger, K., and Harlow, E. (1989) 1160
The human papilloma virus-16 E7 oncoprotein is able to bind to the 1161
retinoblastoma gene product. *Science* 243, 934–937. 1162

- 1163 (12) Munger, K., and Howley, P. M. (2002) Human papillomavirus
1164 immortalization and transformation functions. *Virus Res* 89, 213–228.
- 1165 (13) Munger, K., Werness, B. A., Dyson, N., Phelps, W. C., Harlow, E.,
1166 and Howley, P. M. (1989) Complex formation of human papillomavirus
1167 E7 proteins with the retinoblastoma tumor suppressor gene product.
1168 *EMBO J.* 8, 4099–4105.
- 1169 (14) Heck, D. V., Yee, C. L., Howley, P. M., and Munger, K. (1992)
1170 Efficiency of binding the retinoblastoma protein correlates with the
1171 transforming capacity of the E7 oncoproteins of the human
1172 papillomaviruses. *Proc. Natl. Acad. Sci. U.S.A.* 89, 4442–4446.
- 1173 (15) Crook, T., Morgenstern, J. P., Crawford, L., and Banks, L. (1989)
1174 Continued expression of HPV-16 E7 protein is required for
1175 maintenance of the transformed phenotype of cells co-transformed by
1176 HPV-16 plus EJ-ras. *EMBO J.* 8, 513–519.
- 1177 (16) De Marco, F., Bucay, E., Foppoli, C., Fiorini, A., Blarmino, C., Filipi,
1178 K., Giorgi, A., Schinina, M. E., Di Domenico, F., Coccia, R., Butterfield,
1179 D. A., and Perluigi, M. (2012) Oxidative stress in HPV-driven viral
1180 carcinogenesis: redox proteomics analysis of HPV-16 dysplastic and
1181 neoplastic tissues. *PLoS One* 7, e34366.
- 1182 (17) De Marco, F. (2013) Oxidative stress and HPV carcinogenesis.
1183 *Viruses* 5, 708–731.
- 1184 (18) Williams, V. M., Filipova, M., Soto, U., and Duerksen-Hughes, P.
1185 J. (2011) HPV-DNA integration and carcinogenesis: putative roles for
1186 inflammation and oxidative stress. *Future Virol.* 6, 45–57.
- 1187 (19) Mileo, A. M., Abbruzzese, C., Mattarocci, S., Bellacchio, E.,
1188 Pisano, P., Federico, A., Maresca, V., Picardo, M., Giorgi, A., Maras, B.,
1189 Schinina, M. E., and Paggi, M. G. (2009) Human papillomavirus-16 E7
1190 interacts with glutathione S-transferase P1 and enhances its role in cell
1191 survival. *PLoS One* 4, e7254.
- 1192 (20) Alonso, L. G., Garcia-Alai, M. M., Nadra, A. D., Lapena, A. N.,
1193 Almeida, F. L., Gualfetti, P., and Prat-Gay, G. D. (2002) High-risk
1194 (HPV16) human papillomavirus E7 oncoprotein is highly stable and
1195 extended, with conformational transitions that could explain its multiple
1196 cellular binding partners. *Biochemistry* 41, 10510–10518.
- 1197 (21) Ohlenschlager, O., Seiboth, T., Zengerling, H., Briese, L.,
1198 Marchanka, A., Ramachandran, R., Baum, M., Korbas, M., Meyer-
1199 Klaucke, W., Durst, M., and Gorlach, M. (2006) Solution structure of
1200 the partially folded high-risk human papilloma virus 45 oncoprotein E7.
1201 *Oncogene* 25, 5953–5959.
- 1202 (22) Liu, X., Clements, A., Zhao, K., and Marmorstein, R. (2006)
1203 Structure of the human Papillomavirus E7 oncoprotein and its
1204 mechanism for inactivation of the retinoblastoma tumor suppressor. *J.*
1205 *Biol. Chem.* 281, 578–586.
- 1206 (23) Garcia-Alai, M. M., Alonso, L. G., and de Prat-Gay, G. (2007) The
1207 N-terminal module of HPV16 E7 is an intrinsically disordered domain
1208 that confers conformational and recognition plasticity to the
1209 oncoprotein. *Biochemistry* 46, 10405–10412.
- 1210 (24) Clements, A., Johnston, K., Mazzarelli, J. M., Ricciardi, R. P., and
1211 Marmorstein, R. (2000) Oligomerization properties of the viral
1212 oncoproteins adenovirus E1A and human papillomavirus E7 and their
1213 complexes with the retinoblastoma protein. *Biochemistry* 39, 16033–
1214 16045.
- 1215 (25) Chemes, L. B., Glavina, J., Alonso, L. G., Marino-Buslje, C., de
1216 Prat-Gay, G., and Sanchez, I. E. (2012) Sequence evolution of the
1217 intrinsically disordered and globular domains of a model viral
1218 oncoprotein. *PLoS One* 7, No. e47661.
- 1219 (26) McIntyre, M. C., Frattini, M. G., Grossman, S. R., and Laimins, L.
1220 A. (1993) Human papillomavirus type 18 E7 protein requires intact Cys-
1221 X-X-Cys motifs for zinc binding, dimerization, and transformation but
1222 not for Rb binding. *J. Virol.* 67, 3142–3150.
- 1223 (27) Alonso, L. G., Garcia-Alai, M. M., Smal, C., Centeno, J. M., Iacono,
1224 R., Castano, E., Gualfetti, P., and de Prat-Gay, G. (2004) The HPV16 E7
1225 viral oncoprotein self-assembles into defined spherical oligomers.
1226 *Biochemistry* 43, 3310–3317.
- 1227 (28) Patrick, D. R., Oliff, A., and Heimbrook, D. C. (1994)
1228 Identification of a novel retinoblastoma gene product binding site on
1229 human papillomavirus type 16 E7 protein. *J. Biol. Chem.* 269, 6842–
1230 6850.
- (29) Miseta, A., and Csutora, P. (2000) Relationship between the
occurrence of cysteine in proteins and the complexity of organisms. *Mol.*
Biol. Evol. 17, 1232–1239.
- (30) World Health Organization International Agency for Research on
Cancer (1995) Human papillomavirus. *IARC Monographs on the*
Evaluation of Carcinogenic Risks to Humans, Vol. 64, pp 1–409, World
Health Organization, Geneva.
- (31) Marino, S. M., and Gladyshev, V. N. (2010) Cysteine function
governs its conservation and degeneration and restricts its utilization on
protein surfaces. *J. Mol. Biol.* 404, 902–916.
- (32) Ferrer-Sueta, G., Manta, B., Botti, H., Radi, R., Trujillo, M., and
Denicola, A. (2011) Factors affecting protein thiol reactivity and
specificity in peroxide reduction. *Chem. Res. Toxicol.* 24, 434–450.
- (33) Pace, N. J., and Weerapana, E. (2013) Diverse functional roles of
reactive cysteines. *ACS Chem. Biol.* 8, 283–296.
- (34) Thamsen, M., and Jakob, U. (2011) The redoxome: Proteomic
analysis of cellular redox networks. *Curr. Opin. Chem. Biol.* 15, 113–119.
- (35) Reddie, K. G., and Carroll, K. S. (2008) Expanding the functional
diversity of proteins through cysteine oxidation. *Curr. Opin. Chem. Biol.*
12, 746–754.
- (36) Pimentel, D., Haeussler, D. J., Matsui, R., Burgoyne, J. R., Cohen,
R. A., and Bachschmid, M. M. (2012) Regulation of cell physiology and
pathology by protein S-glutathionylation: lessons learned from the
cardiovascular system. *Antioxid. Redox Signal.* 16, 524–542.
- (37) Anathy, V., Roberson, E. C., Guala, A. S., Godburn, K. E., Budd, R.
C., and Janssen-Heininger, Y. M. (2012) Redox-based regulation of
apoptosis: S-glutathionylation as a regulatory mechanism to control cell
death. *Antioxid. Redox Signal.* 16, 496–505.
- (38) Tanner, J. J., Parsons, Z. D., Cummings, A. H., Zhou, H., and
Gates, K. S. (2011) Redox regulation of protein tyrosine phosphatases:
structural and chemical aspects. *Antioxid. Redox Signal.* 15, 77–97.
- (39) Neumann, C. A., Cao, J., and Manevich, Y. (2009) Peroxiredoxin
1 and its role in cell signaling. *Cell Cycle* 8, 4072–4078.
- (40) Bulaj, G., Kortemme, T., and Goldenberg, D. P. (1998)
Ionization-reactivity relationships for cysteine thiols in polypeptides.
Biochemistry 37, 8965–8972.
- (41) Gilbert, H. F. (1995) Thiol/disulfide exchange equilibria and
disulfide bond stability. *Methods Enzymol.* 251, 8–28.
- (42) Laemmli, U. K. (1970) Cleavage of structural proteins during the
assembly of the head of bacteriophage. *Nature* 227, 680–685.
- (43) Hunt, J. B., Neece, S. H., and Ginsburg, A. (1985) The use of 4-(2-
pyridylazo)resorcinol in studies of zinc release from *Escherichia coli*
aspartate transcarbamoylase. *Anal. Biochem.* 146, 150–157.
- (44) Ellman, G., and Lysko, H. (1979) A precise method for the
determination of whole blood and plasma sulfhydryl groups. *Anal.*
Biochem. 93, 98–102.
- (45) Chemes, L. B., Sanchez, I. E., Smal, C., and de Prat-Gay, G. (2010)
Targeting mechanism of the retinoblastoma tumor suppressor by a
prototypical viral oncoprotein. Structural modularity, intrinsic disorder
and phosphorylation of human papillomavirus E7. *FEBS J.* 277, 973–
988.
- (46) Edgar, R. C. (2004) MUSCLE: multiple sequence alignment with
high accuracy and high throughput. *Nucleic Acids Res.* 32, 1792–1797.
- (47) Sali, A., and Blundell, T. L. (1993) Comparative protein
modelling by satisfaction of spatial restraints. *J. Mol. Biol.* 234, 779–815.
- (48) Eswar, N., Webb, B., Marti-Renom, M. A., Madhusudhan, M. S.,
Eramian, D., Shen, M. Y., Pieper, U., and Sali, A. (2006) Comparative
protein structure modeling using Modeller, in *Current Protocols in*
Bioinformatics (Baxevanis, D., et al., Eds.) Chapter 5, Unit 5.6, Wiley,
New York.
- (49) Kabsch, W., and Sander, C. (1983) Dictionary of protein
secondary structure: pattern recognition of hydrogen-bonded and
geometrical features. *Biopolymers* 22, 2577–2637.
- (50) Morgan, B., Ezerina, D., Amoako, T. N., Riemer, J., Seedorf, M.,
and Dick, T. P. (2013) Multiple glutathione disulfide removal pathways
mediate cytosolic redox homeostasis. *Nat. Chem. Biol.* 9, 119–125.
- (51) Veal, E. A., Day, A. M., and Morgan, B. A. (2007) Hydrogen
peroxide sensing and signaling. *Mol. Cell* 26, 1–14.

- 1299 (52) Stadtman, E. R., and Berlett, B. S. (1998) Reactive oxygen-
1300 mediated protein oxidation in aging and disease. *Drug Metab. Rev.* 30,
1301 225–243.
- 1302 (53) Chemes, L. B., Sanchez, I. E., and de Prat-Gay, G. (2011) Kinetic
1303 recognition of the retinoblastoma tumor suppressor by a specific protein
1304 target. *J. Mol. Biol.* 412, 267–284.
- 1305 (54) Shevchenko, A., Tomas, H., Havlis, J., Olsen, J. V., and Mann, M.
1306 (2006) In-gel digestion for mass spectrometric characterization of
1307 proteins and proteomes. *Nat. Protoc.* 1, 2856–2860.
- 1308 (55) Phelps, W. C., Munger, K., Yee, C. L., Barnes, J. A., and Howley, P.
1309 M. (1992) Structure-function analysis of the human papillomavirus type
1310 16 E7 oncoprotein. *J. Virol.* 66, 2418–2427.
- 1311 (56) Todorovic, B., Massimi, P., Hung, K., Shaw, G. S., Banks, L., and
1312 Mymryk, J. S. (2011) Systematic analysis of the amino acid residues of
1313 human papillomavirus type 16 E7 conserved region 3 involved in
1314 dimerization and transformation. *J. Virol.* 85, 10048–10057.
- 1315 (57) Dong, W. L., Caldeira, S., Sehr, P., Pawlita, M., and Tommasino,
1316 M. (2001) Determination of the binding affinity of different human
1317 papillomavirus E7 proteins for the tumour suppressor pRb by a plate-
1318 binding assay. *J. Virol. Methods* 98, 91–98.
- 1319 (58) Ruden, D. M., Garfinkel, M. D., Sollars, V. E., and Lu, X. (2003)
1320 Waddington's widget: Hsp90 and the inheritance of acquired characters.
1321 *Sem. Cell Dev. Biol.* 14, 301–310.
- 1322 (59) Jakob, U., Eser, M., and Bardwell, J. C. (2000) Redox switch of
1323 hsp33 has a novel zinc-binding motif. *J. Biol. Chem.* 275, 38302–38310.
- 1324 (60) Jakob, U., Muse, W., Eser, M., and Bardwell, J. C. (1999)
1325 Chaperone activity with a redox switch. *Cell* 96, 341–352.
- 1326 (61) Bourles, E., Isaac, M., Lebrun, C., Latour, J. M., and Seneque, O.
1327 (2011) Oxidation of Zn(Cys)₄ zinc finger peptides by O₂ and H₂O₂:
1328 products, mechanism and kinetics. *Chemistry* 17, 13762–13772.
- 1329 (62) Christman, M. F., Storz, G., and Ames, B. N. (1989) OxyR, a
1330 positive regulator of hydrogen peroxide-inducible genes in *Escherichia*
1331 *coli* and *Salmonella typhimurium*, is homologous to a family of bacterial
1332 regulatory proteins. *Proc. Natl. Acad. Sci. U.S.A.* 86, 3484–3488.
- 1333 (63) Choi, H., Kim, S., Mukhopadhyay, P., Cho, S., Woo, J., Storz, G.,
1334 and Ryu, S. E. (2001) Structural basis of the redox switch in the OxyR
1335 transcription factor. *Cell* 105, 103–113.
- 1336 (64) Littler, D. R., Harrop, S. J., Fairlie, W. D., Brown, L. J., Pankhurst,
1337 G. J., Pankhurst, S., DeMaere, M. Z., Campbell, T. J., Bauskin, A. R.,
1338 Tonini, R., Mazzanti, M., Breit, S. N., and Curmi, P. M. (2004) The
1339 intracellular chloride ion channel protein CLIC1 undergoes a redox-
1340 controlled structural transition. *J. Biol. Chem.* 279, 9298–9305.
- 1341 (65) Marino, S. M., and Gladyshev, V. N. (2012) Analysis and
1342 functional prediction of reactive cysteine residues. *J. Biol. Chem.* 287,
1343 4419–4425.
- 1344 (66) Choi, J., Choi, S., Choi, J., Cha, M. K., Kim, I. H., and Shin, W.
1345 (2003) Crystal structure of *Escherichia coli* thiol peroxidase in the
1346 oxidized state: insights into intramolecular disulfide formation and
1347 substrate binding in atypical 2-Cys peroxiredoxins. *J. Biol. Chem.* 278,
1348 49478–49486.
- 1349 (67) Hall, A., Nelson, K., Poole, L. B., and Karplus, P. A. (2011)
1350 Structure-based insights into the catalytic power and conformational
1351 dexterity of peroxiredoxins. *Antioxid. Redox Signal.* 15, 795–815.
- 1352 (68) Fomenko, D. E., and Gladyshev, V. N. (2003) Identity and
1353 functions of CxxC-derived motifs. *Biochemistry* 42, 11214–11225.